Stable isotope probing and metagenomics highlight the effect of plants on uncultured phenanthrene-degrading bacterial consortium in polluted soil

François Thomas, Erwan Corre, Aurélie Cebron

Stable isotope probing and metagenomics highlight the effect of plants on uncultured phenanthrene-degrading bacteria in polluted soil

Running title: Phenanthrene degraders in bare vs. planted soil

François THOMAS[1,2], Erwan CORRE[3], Aurélie CEBRON[1†]

[1] Université de Lorraine, CNRS, LIEC 54500 Nancy, France

[2] Sorbonne Université, CNRS, Integrative Biology of Marine Models (LBI2M), Station Biologique de Roscoff (SBR), 29680 Roscoff, France

[3] CNRS, Sorbonne Université, FR2424, ABiMS, Station Biologique de Roscoff, 29680, Roscoff, France

[†] Corresponding author: aurelie.cebron@univ-lorraine.fr; Full postal address: LIEC UMR7360, Faculté des Sciences et technologie, Bd des Aiguillettes, BP70239, 54506 Vandoeuvre-les-Nancy, France. Phone: (+33) 372745215.

ISME J sections: Microbial ecology and functional diversity of natural habitats

Abstract

Polycyclic aromatic hydrocarbons (PAHs) are ubiquitous soil pollutants. The discovery that plants can stimulate microbial degradation of PAHs promoted research on rhizoremediation strategies. We combined DNA-SIP with metagenomics to assess the influence of plants on the identity and metabolic functions of active PAH-degrading bacteria in contaminated soil, using phenanthrene (PHE) as a model hydrocarbon. ^{13}C-PHE dissipation was 2.5-fold lower in ryegrass-planted conditions than in bare soil. Metabarcoding of 16S rDNA from bare and planted conditions revealed respectively 130 and 73 OTUs significantly enriched in ^{13}C-SIP incubations compared to ^{12}C-controls. Active PHE-degraders were taxonomically diverse (*Proteobacteria*, *Actinobacteria* and *Firmicutes*), with *Sphingomonas* and *Sphingobium* dominating in bare and planted soil, respectively. Metagenomes of ^{13}C-enriched DNA fractions contained more genes involved in aromatic compounds metabolism in bare soil, whereas carbohydrate catabolism genes were more abundant in planted soil. Functional gene

annotation allowed reconstructing complete pathways for PHE catabolism. *Sphingomonadales* were the major taxa performing the first steps of PHE degradation in both conditions, suggesting their critical role to initiate *in-situ* PAH remediation. Analysis of metagenomic bins from ^{13}C-enriched *Sphingomonas* and *Sphingobium* highlighted different metabolic strategies, the latter containing less PAH-degrading genes but a more diverse repertoire of carbohydrate active enzymes potentially targeting plant root material.

Introduction

Polycyclic aromatic hydrocarbons (PAHs) are ubiquitous soil pollutants with environmental and public health concerns [1]. PAHs released into the environment by industrial activities can be removed through physical, chemical and biological processes [2]. Microorganisms that use PAHs as carbon sources play essential roles in natural attenuation of pollutants in contaminated ecosystems [3]. Numerous PAH catabolic pathways are described in bacteria, archaea and fungi, including both aerobic and anaerobic processes [1,3]. Several studies have evidenced an increased microbial degradation of PAHs in the presence of plants [4,5]. The discovery of this "rhizosphere effect" promoted the development of rhizoremediation strategies to treat PAH-contaminated soils [6,7]. However, literature shows contrasting results with no rhizosphere effect or even a negative influence on PAH-degradation efficiency [8,9]. These discrepancies may reflect the use of different model plants, soil types, indigenous microorganisms [10] and types of PAHs [11]. Such variations may also result from temporal variations in rhizospheric processes during plant development. We previously showed that phenanthrene degradation was slowed down during the early development of ryegrass [12], a plant commonly used in PAH rhizoremediation studies [13]. Differences in PAH-degradation with or without plants could be explained by the selection of two distinct PAH-degrading bacterial populations. Indeed, active bacterial populations were different in soil supplemented or not with root exudates [14] and in planted or bare soil microcosms [12]. Plant roots exude labile carbon sources that can be preferentially degraded by rhizospheric microbial communities to the detriment of PAH dissipation [9]. Therefore, investigation of PAH-degraders in the rhizosphere of contaminated soils is needed to decipher the influence of plants and ultimately improve PAH biodegradation efficiency. One challenge is to specifically target microorganisms actively degrading PAHs in polluted soils, without the cultivation bias. DNA-Stable Isotope Probing (DNA-SIP) is a powerful technique for linking functions with identity of uncultured microorganisms in complex microbiota. Approaches combining DNA-SIP and metagenomics are increasingly used to investigate microbial communities involved in

anthropogenic compound biodegradation [15,16]. To date DNA-SIP has been successfully applied to identify soil bacteria that metabolize PAHs such as naphthalene [17,18,19,20], phenanthrene [14,18,21,22,23,24,25,26], anthracene [24,27,28], fluoranthene [24], pyrene [29,30] and benzo[a]pyrene [31]. DNA-SIP has also been used to explore PAH-degraders in the presence of purified root exudates [14] and to identify degraders of root exudates in the rhizosphere [32]. However, we still lack a comprehensive view on the major microbial actors of PAH degradation and their catabolic pathways in contaminated soils, and how it changes in the presence of plants.

In this study we investigated PAH-degrading bacteria of a historically polluted soil, using ^{13}C-labelled phenanthrene (PHE) as a metabolic tracer. We combined DNA-SIP with metagenomics to assess for the first time the influence of plant rhizosphere on the diversity, identity and metabolic functions of bacteria actively involved in phenanthrene degradation.

Material and Methods

Soil sample and phenanthrene spiking

Soil was collected from a former coking plant site (NM soil, Neuves-Maisons, France), dried at room temperature, sieved to 2 mm and stored in the dark at room temperature until experimental set-up. PAH contamination dates back ca. 100 years and reaches 1 260 mg Σ16PAHs.kg^{-1}. Other soil characteristics were detailed elsewhere [33]. For spiking, two batches of soil were recontaminated at 2 500 mg.kg^{-1} respectively with [U-$^{13}C_{14}$]-labeled phenanthrene (Sigma-Aldrich Isotec, St Louis, USA) and unlabeled ^{12}C-PHE (Fluka). Ten grams of dry soil were mixed with 2.5 ml of PHE stock solutions (10 mg.ml^{-1} in hexane). After complete solvent evaporation, aliquots of 1.1 g recontaminated soil were mixed with 9.9 g of non-recontaminated soil (1:10 dilution) to obtain a final concentration of fresh PHE of 250 mg.kg^{-1}.

SIP incubations

SIP incubations were performed using previously described two-compartment microcosms [12]. Eight ryegrass seedlings (*Lolium multiflorum*, Italian ryegrass, Podium variety, LG seeds, France) were allowed to grow for 21 days until roots reached the bottom of the first compartment containing 30 g of non-recontaminated NM soil and maintained at 80% of the

soil water-holding capacity in a growth chamber (22°C /18°C day/night, 80% relative humidity, c.a. 250 µmol photons m^{-2} s^{-1}, 16 hours photoperiod). A second compartment containing 10 g of ^{12}C or ^{13}C PHE-spiked soil was then appended below the first one to allow root colonization in the growth chamber. After 10 days, soil from the second compartment was retrieved in a glass Petri dish. Roots were removed using a brush and tweezers. Aliquots of soil were collected in glass vials for organic extraction and isotopic analysis; the rest was stored in plastic vial and immediately frozen in liquid nitrogen for further nucleic acid extraction. All samples were stored at -80°C until analysis. Non-vegetated ("bare") microcosms were handled in the same way, except no ryegrass was planted in the first compartment. Independent triplicates were performed for the four conditions (i.e. ^{12}C-bare, ^{12}C-planted, ^{13}C-bare and ^{13}C-planted), for a total of 12 microcosms. Aerial plant biomass was harvested, ground in liquid nitrogen, dried at 60°C and stored at room temperature. To capture the initial PHE concentration, an additional set of second compartments was prepared and sacrificed within 2 hours.

Organic extraction and phenanthrene quantification

Lyophilized soil was pulverized in a mixer mill (MM200, Retsch). Soil samples (250 mg) were mixed with 1 g activated copper and 2 g anhydrous Na_2SO_4 and extracted with dichloromethane (DCM) using an high pressure and temperature automated extractor Dionex ASE350 as described elsewhere [34]. Post-extraction soil residues were recovered for isotopic analysis. DCM extracts were analyzed by gas chromatography coupled to mass spectrometry (GC-MS) [35].

The ^{13}C content coming from the added ^{13}C-PHE was expressed as $^{13}C_{sample} = \alpha \times PHE_{sample}$, where PHE_{sample} is the PHE content ($mg.kg^{-1}$) and α the massic proportion of carbon atoms in PHE molecule (0.9434). The proportion of ^{13}C remaining compared to the amount added initially was expressed as $100 \times {}^{13}C_{sample\ D10}/{}^{13}C_{sample\ D0}$. D0 was the initial measure and D10 after 10 days.

Isotopic analysis

Isotopic composition of soil samples and post-extraction soil residues, dry DCM extracts and aerial plant biomass was determined at the INRA PTEF (Champenoux, France) using Elemental analyzer (vario ISOTOPE cube, Elementar, Hanau, Germany) interfaced in line with a gas isotope ratio mass spectrometer (IsoPrime 100, Isoprime Ltd, Cheadle, UK). Carbon isotopic composition was expressed as $\delta^{13}C$ (‰) versus Vienna PeeDee Belemnite

(V-PDB). The ratio of ^{13}C versus ^{12}C in samples was expressed as $R_{sample} = R_{V\text{-}PDB} \times (1 + \delta^{13}C_{sample}/1000)$, where $R_{V\text{-}PDB} = {}^{13}C_{V\text{-}PDB}/{}^{12}C_{V\text{-}PDB} = 0.0112375$. The proportion of ^{13}C in a sample compared to the amount initially added from ^{13}C-PHE was calculated as $(R_{sample\ D10} - R_{matrix})/(R_{sample\ D0} - R_{matrix})$, where R_{matrix} is the natural $^{13}C/^{12}C$ ratio of the NM soil, DCM extracts or soil residues (average 0.01085).

DNA extraction and isopycnic separation

DNA was extracted from 0.5 g of soil using the Fast DNA Spin Kit for Soil (MP Biomedicals, France). Five replicate extractions were pooled for each sample. DNA was quantified using the Quant-iT Picogreen dsDNA assay kit (Invitrogen). Isopycnic separation of ^{12}C- and ^{13}C-labeled DNA ("light" and "heavy" DNA, respectively) was performed as described previously [36]. DNA (3.9 µg) was mixed in 5.1 ml tubes with CsCl solution and gradient buffer to a final density of 1.725 $g.ml^{-1}$. Ultracentrifugation was performed in a vertical rotor (VTi 65.2, Beckman), at 15°C, 176 985***g*** for 40 h (INRA, Champenoux). Thirteen fractions (ca. 400 µl) were collected per tube and weighed on a digital balance (precision 10^{-4} g) to confirm gradient formation. DNA was precipitated with 800 µl polyethylene glycol 6000 (1.6 M) and 2 µl polyacryl carrier (Euromedex) overnight at room temperature, recovered by centrifugation 45 min at 13 000***g*** and washed once with 500 µl 70% (v/v) ethanol. Pellets were dried for 2 min in a vacuum concentrator (Centrivap Jouan RC1010, ThermoScientific), resuspended in 30 µl molecular-biology grade water (Gibco, Life Technologies) and stored at -20°C.

Real-time quantitative PCR (qPCR)

Bacterial 16S, Archaeal 16S and fungal 18S rRNA gene copies were quantified using the primer pairs 968F/1401R [37], 571F/910R [38] and FF390R/Fung5F [39,40]. qPCR reactions (20µl) were performed as described previously [41] on a CFX96 real-time system (BioRad) and contained 1X iQ SybrGreen Super Mix (BioRad), 12 µg bovine serum albumin, 0.2 µl dimethyl sulfoxide, 40 µg of T4 bacteriophage gene 32 product (MP Biomedicals, France), 1 µl of template (DNA or 10-fold linearized standard plasmid dilution series from 10^8 to 10^2 gene copies.μl^{-1}) and 8 pmol of each primer. Reactions were heated at 95°C for 5 min, followed by 45 cycles of 30 s at 95°C, 30 s at 56°C for bacterial 16S rRNA, 60°C for archaeal 16S rRNA or 50°C for 18S rRNA, 30 s at 72°C and 10 s at 82°C to capture the fluorescence signal while dissociating primer dimers. Dissociation curves were obtained by heating

reactions from 50 to 95 °C. Fractions identified as containing "heavy" DNA were pooled and quantified by Picogreen assay.

16S rRNA gene amplicon sequencing and analysis

Fragments of 430 bp covering the V3/V4 region of bacterial 16S rRNA genes were amplified from 12 samples of "heavy" DNA recovered from ^{13}C-SIP and ^{12}C-control samples and sequenced as described previously [12] with a dual-index paired-end strategy [42]. Amplicons were obtained by 28 cycles of PCR using Accuprime Super Mix (Invitrogen) on 1 µl template DNA, purified using the UltraClean-htp 96 Well PCR Clean-Up kit (MOBIO) and quantified by Picogreen assay. An equimolar pool at 10 nM was purified using Nucleospin PCR Clean-Up kit (Macherey-Nagel) and sequenced on a single lane of Illumina Miseq PE250 at the Georgia Genomics Facility (Athens, GA, USA). Paired-end reads were trimmed to a minimum Qscore of 20, joined with Pandaseq [43] and filtered for length in the 400-450 bp range with no ambiguous bases. Sequence data were analyzed as described previously [12] in QIIME v1.9 [44] with chimera detection and clustering in Operational Taxonomic Units (OTUs) at 97% using UCHIME and USEARCH v6.1, respectively [45, 46], followed by taxonomy assignment using the RDP classifier [47] with the Greengenes database v13_8 [48]. After removal of chloroplasts and mitochondria OTUs, datasets were rarefied to the lowest number of sequences per sample (9 532 sequences). To identify OTUs significantly enriched in ^{13}C-SIP incubations compared to ^{12}C-controls, a subset of data was produced to keep only OTUs (i) represented by at least 5 sequences in each triplicate ^{13}C-SIP sample and (ii) with an average abundance higher in ^{13}C-SIP samples compared to ^{12}C-controls. This subset was then log-transformed and compared using Welch's test with Benjamini-Hochberg correction of the p-value performed in R v3.1.3 [49], separately for bare and planted samples.

Shotgun metagenomic sequencing and analysis

"Heavy" DNA recovered from the six ^{13}C-SIP samples was sequenced on 3 lanes of Illumina MiSeq PE300 at the Georgia Genomics Facility (Athens, GA, USA). Adapters removal and quality filtering was performed on raw reads using Trimmomatic [50] with the following parameters: remove adapters (ILLUMINACLIP:adapters.fa:2:30:10), trim 5'- or 3'-bases if phred Qscore <25 (LEADING:25 TRAILING:25), trim read when average quality < 25 (SLIDINGWINDOW:4:25) and discard reads shorter than 100 bp (MINLEN:100). Based on FastQC report, paired and unpaired reads 2 obtained after Trimmomatic were further cropped at 250 and 230 bp, respectively. Unassembled DNA sequences were uploaded to MG-RAST

[51] and compared to the Subsystems database (November 2017) with default parameters. Proportions in functional profiles were compared using Welch's two-sided test with Benjamini-Hochberg correction. Raw metagenomic reads were assembled separately for each sample using SPAdes v3.7.0 [52], with the –meta option and testing kmer sizes of 21, 33, 55, 77 ,99 and 127. Taxonomic assignment of assembled contigs longer than 5 kb was performed using PhyloPythiaS [53]. Genomic features on assembled contigs were predicted and annotated using prokka v1.12 [54]. Predicted genomic features were also screened for functional genes encoding enzymes potentially involved in aerobic degradation of aromatic compounds using AromaDeg [55], with minimum BLAST homology of 50% and minimum alignment length of 150 bp. Sequences of selected AromaDeg enzyme families were further aligned using MAFFT [56] with the L-INS-i method. Alignments were manually edited in JalView [57] and used for maximum-likelihood phylogenetic tree construction in MEGA v6 [58] after selection of the best protein model. Genes encoding putative carbohydrate active enzymes (CAZymes) were annotated using dbcan [59]. The GhostKOALA annotation server [60] was used to assign KEGG orthologies to genes in the metagenomes and reconstruct metabolic pathways.

Data access

16S rRNA gene amplicon sequences are available at NCBI under BioProject ID PRJNA485442 (BioSamples: SAMN09791490-SAMN09791501). Raw and assembled shotgun metagenomics data are available on MG-RAST under study name RHIZORG_WGS and RHIZORG_ASSEMBLED, respectively.

Results

Fate of phenanthrene

The fate of spiked PHE was followed in total soil, organic extracts and soil residues after extraction (**Table 1**). No decrease in ^{13}C content was observed in total soil over the 10 days period. The proportion of ^{13}C remaining in DCM extracts (containing PAHs) decreased of ca. 25% in bare soil and only 10% in planted soil (Welch t-test P=0.06). Consistency between AE-IRMS and GC-MS results indicates that most of the DCM-extractable ^{13}C was ^{13}C-PHE, without major contributions of ^{13}C-labeled degradation products. At Day 0, 3.5% of the spiked ^{13}C was already non-extractable with DCM and recovered in soil residues, suggesting

a rapid sequestration of PHE on soil particles. After 10 days, this non-extractable fraction reached 13% and 5.8% in bare and planted microcosms, respectively (Student t-test, $P<0.001$). This increase likely reflects the incorporation of ^{13}C in microbial biomass, and the production of ^{13}C-labeled hydrophilic intermediates that were not extracted with DCM. Aerial plant biomass was only weakly enriched in ^{13}C (0.048% ^{13}C content increase compared to ^{12}C-controls).

Taxonomic characterization of active PHE degraders

Community gDNA extracted from ^{12}C-controls and ^{13}C-SIP incubations was separated by isopycnic centrifugation and fractionated. Quantification of bacterial 16S rRNA genes showed a 6-fold increase in fractions 6-8 (buoyant density 1.713-1.727 $g.ml^{-1}$) of ^{13}C-SIP bare microcosms compared to ^{12}C-controls (**Figure S1A**). This increase was only 2-fold in planted microcosms (**Figure S1B**), suggesting a lower incorporation of ^{13}C within bacterial biomass in the presence of ryegrass. Archaeal and fungal rRNA genes were not enriched in any fractions from ^{13}C-SIP compared to ^{12}C-controls (not shown), suggesting that Archaea and Fungi did not metabolize a significant proportion of PHE in the tested conditions. Fractions 6-8 from each sample were pooled (hereafter "heavy DNA") and analyzed by high-throughput sequencing of the 16S rRNA genes. We obtained a total of 405 345 quality-filtered paired-end 16S rDNA sequences from the 12 samples, ranging from 9 532 to 52 544 sequences per sample. Based on rarefied dataset, sequences were clustered in 5 690 OTUs at 97% identity. The taxonomic affiliation of OTUs differed between heavy DNA fractions of ^{13}C-SIP incubations and ^{12}C-controls in both bare and planted conditions (**Figure 1A**). We detected 130 and 73 OTUs significantly enriched in ^{13}C-SIP incubations compared to ^{12}C-controls in bare and planted conditions, respectively, with 40 OTUs shared between the two conditions (**Figure 1B**). These active PHE-degrading OTUs were affiliated to *Actinobacteria*, *Alpha-*, *Beta-* and *Gammaproteobacteria* in both conditions, while *Firmicutes* were only enriched in heavy DNA fractions from bare soil. *Arthrobacter*, unknown *Sphingomonadaceae* and *Gammaproteobacteria* "PYR10d3" were present at a similar level in both conditions. PHE-degrading *Sphingomonas* and *Alcaligenaceae* OTUs were favored in bare soil compared to planted condition. Conversely, *Sphingobium* and unknown *Micrococcaceae* were more represented in planted condition. In each condition, one genus dominated the PHE-degrading population. Namely, *Sphingomonas* dominated in bare soil (43% of total sequences and 61% of total OTUs), while *Sphingobium* prevailed in planted soil (28% of total sequences, 41% of total OTUs).

Functional profiling of ^{13}C-labeled metagenomes

A total of ~90 million paired-end reads representing 17.6 Gb sequence data were obtained for the six heavy DNA samples from ^{13}C-SIP incubations (**Table S1**). MG-RAST analysis showed that 14 of the 28 functional categories were differentially represented in the two conditions (**Figure 2A**). The greatest differences between bare and planted conditions were found for the two categories: "Carbohydrates" (8.63% and 10.61% in bare and planted soil ^{13}C-metagenomes, respectively; q-value=0.016) and "Metabolism of aromatic compounds" (4.66% and 2.45% in bare and planted soil ^{13}C-metagenomes, respectively; q-value=0.015). Within the category "Carbohydrates" (**Figure 2B**), the abundance of gene sequences affiliated to the metabolism of polysaccharides, monosaccharides, fermentation, di- and oligosaccharides, central carbohydrates and aminosugars, were all significantly over-represented in the planted soil ^{13}C-metagenomes. Within the category "Metabolism of aromatic compounds" (**Figure 2C**), sequences matching the anaerobic degradation genes were detected in identical relative abundance between the two conditions. The genes belonging to the three other sub-categories, i.e. peripheral pathways for catabolism of aromatic compounds, metabolism of central aromatic intermediates, and other, were significantly over-represented in bare soil ^{13}C-metagenomes.

Genes encoding enzymes potentially involved in aerobic degradation of aromatic compounds were detected in assembled metagenomes using AromaDeg, and their prevalence was calculated relative to the single-copy gene *recA* (**Table 2**). A significantly lower prevalence of genes encoding benzoate oxygenases, biphenyl oxygenases, extradiol dioxygenases of the vicinal oxygen chelate superfamily, homoprotocatechuate oxygenases and salicylate oxygenases was found in ^{13}C-enriched metagenomes from planted condition compared to bare soil. We further analyzed selected members of two enzyme families involved in the first steps of PAH degradation, namely the biphenyl/naphthalene family of Rieske non-heme iron oxygenases and extradiol dioxygenases of the vicinal oxygen chelate family (EXDO I). The biphenyl/naphthalene family comprises most of the dioxygenases reported to date to activate PAHs for further aerobic degradation, whereas the EXDO I family comprises enzymes that fission the ring of pre-activated mono- or polyaromatic derivatives [55]. We notably detected 66 and 20 ORFs encoding oxygenases of the biphenyl/naphthalene family from *Proteobacteria* (Clusters XXIV and XXVI) or *Actinobacteria* (Clusters I, II and V), respectively, as well as 46 ORFS encoding proteobacterial EXDOs preferring bicyclic substrates related to dihydroxynaphthalene dioxygenases (Cluster XII). Phylogenetic analysis

of biphenyl/naphthalene oxygenases from *Proteobacteria* (**Figure 3A**) revealed that the vast majority (56/66) was closely related to known sequences from *Sphingomonas*, *Sphingobium* and *Novosphingobium* with equal distributions between bare and planted soil. Few additional sequences were related to *Cycloclasticus*, *Burkholderia* or *Acidovorax* spp. No sequences were affiliated to *Pseudomonas*. Within *Actinobacteria* (**Figure 3B**), 12 biphenyl/naphthalene dioxygenases were closely related to sequences from *Arthrobacter phenanthrenivorans* (Cluster II) and *Arthrobacter keyseri* (Cluster V). In planted conditions only, 4 additional sequences related to *Mycobacterium* and *Terrabacter* were detected in Cluster V, as well as 2 more divergent sequences. In Cluster XII of the EXDO I family (**Figure 4**), most detected sequences grouped with known proteins from *Sphingomonas*, *Sphingobium* and *Novosphingobium*. Among these, a relatively divergent clade of 20 sequences emerged, with more detected members in bare soil compared to planted conditions. Finally, few additional EXDO I Cluster XII sequences were related to *Sphingopyxis*, *Pseudomonas*, *Acidovorax* or *Burkholderia*.

Reconstruction of phenanthrene degradation pathways

Combining results of the above AromaDeg analysis and the GhostKOALA annotation pipeline, we reconstructed both the O-phthalate/protocatechuate pathway leading to the 3-oxoadipate, as well the naphthalene pathway leading to salicylate (**Figure 5**). GhostKOALA failed to recognize genes involved in the first steps of PHE degradation that were detected with AromaDeg, likely because the KEGG database only contains *nahAc* and *nidA* genes from *Pseudomonas* and *Mycobacterium*, respectively. Salicylate could be converted to gentisate or catechol, being further degraded through ortho- and meta-cleavage pathways leading to intermediates of the TCA cycle. All genes involved in these pathways were present in both conditions. Sequences affiliated to *Sphingomonadales* dominated the early steps of degradation leading to 1-hydroxy-2-naphthaldehyde and pyruvate, as well as later reactions converting naphthalene-1,2-diol to salicylaldehyde and pyruvate. Genes involved in the downstream conversion to gentisate were mainly detected from *Betaproteobacteria* (including *Alcaligenaceae*) and *Sphingomonadales*. Genes annotated in the meta- and ortho-cleavage pathways for catechol utilization were taxonomically more diverse, with sequences affiliated to *Alpha-*, *Beta-* and *Gammaproteobacteria*, *Actinobacteria* and *Firmicutes*. Overall, *Actinobacteria* and *Firmicutes* had higher contributions to the phthalate and protocatechuate pathway than the naphthalene and salicylate pathway.

Focus on *Sphingomonas* and *Sphingobium* metagenomes

We further focused on the two dominant PHE-degrading populations of *Sphingomonas* and *Sphingobium* identified in bare and planted soil through SIP (**Figure 1B**). After taxonomic affiliation of contigs larger than 5 kb, the best metagenome assemblies were obtained for *Sphingomonas* population in bare soil and *Sphingobium* population in planted soil, respectively, with maximum contig size larger than 1 Mb (**Supplementary Table S2**). The *Sphingobium* metagenome from bare soil was more fragmented (average size 71 kb, maximum size 278 kb). This likely reflects a lower coverage of the *Sphingobium*-affiliated sequences in ^{13}C-enriched metagenomes and corroborates the lower success of this PHE-degrading genus in bare soil compared to planted conditions. The single-copy RecA protein of ^{13}C-enriched metagenomes of *Sphingomonas* was identical in the 3 bare soil microcosms and had its best blastp hit (91% identity) against *Sphingomonas* sp. MM-1 [61], while that of *Sphingobium* was identical in the 3 planted microcosms and had its best blastp hit (100% identity) against *Sphingobium herbicidovorans* NBRC 16415 [62] and *Sphingobium* sp. MI1205 [63]. Functional gene annotation revealed a large arsenal of dioxygenases and monooxygenases with some that could have potential activity on aromatic compounds in *Sphingomonas* metagenomes from bare soil (**Supplementary Table S3**), often grouped in genomic regions. The potential for aromatic compounds degradation was much more restricted in *Sphingobium* metagenomes from planted conditions. We then hypothesized that the greater success of *Sphingobium* PHE-degraders compared to *Sphingomonas* in planted conditions might not be directly due to aromatic compound catabolism, but rather to a more efficient use of plant-derived carbon sources. To test this hypothesis, we screened the metagenomes for genes encoding carbohydrate active enzymes (CAZymes) in the groups carbohydrate esterases (CE), glycoside hydrolases (GH) and polysaccharide lyases (PL) (**Table 3**). Similar numbers of CAZymes were detected in *Sphingomonas* (36 to 47 total CAZymes) and *Sphingobium* (46 to 48 total CAZymes). However, a larger diversity of CAZy families was found in *Sphingobium* (27 different families) than in *Sphingomonas* (19 to 21) metagenomes. Families detected only in *Sphingobium* metagenomes include enzymes potentially involved in plant cell wall breakdown, including the degradation of xylan (CE6, CE7, GH10, GH115, GH43_12, GH67), pectin (PL1_2) and other cell wall compounds (GH16), as well as in the use of disaccharides (maltose, trehalose) that are found in root exudates (GH65). Furthermore, the prevalence of three additional families also potentially involved in plant cell wall breakdown was higher in *Sphingobium* metagenomes compared to *Sphingomonas* (GH13, GH3, PL22).

Discussion

Phenanthrene is often highly concentrated in PAH-contaminated environments and is a model for research on PAH catabolism [1]. We used DNA-SIP to investigate the diversity and metabolic potential of microorganisms involved in phenanthrene degradation in historically contaminated soil. We further assessed the influence of ryegrass, a plant commonly used in phytoremediation studies on PAH-contaminated soils [2,11,64]. To our knowledge, this study is the first to use DNA-SIP combined to metagenomics to assess the influence of plants on bacteria actively involved in phenanthrene degradation in polluted soils. Here, we showed a decreased dissipation rate of phenanthrene in the ryegrass rhizosphere, corroborating previous results [12,14]. The rhizosphere environment contains higher nutrient concentration than the surrounding bulk soil due to root exudates, comprising an array of organic compounds including carbohydrates, amino acids, proteins, flavonoids, aliphatic acids, organic acids and fatty acids [10,32]. Excessive nutrient availability can inhibit the biodegradation of pollutants [65,66,67]. Thus, rhizospheric bacteria may preferentially use labile carbon sources from exudates, leading to slower phenanthrene degradation. The phenanthrene degradation rates we observed (20% and 10% in bare and planted soil in 10 days, respectively) were lower than previous reports, e.g. 60 to 70% PHE degradation in 9 days [21,24] or 68% in 12 days [14]. This discrepancy might be linked to the more realistic conditions of the present experimental setup within a genuine plant rhizosphere, allowing constant input of rhizodeposits during the 10-days time course. The limited dissipation of ^{13}C-PHE after 10 days minimized the risk of cross-feeding, ensuring that ^{13}C-labeled microorganisms are the primary degraders of phenanthrene in the NM soil.

The active ^{13}C-PHE-degrading OTUs belonged to similar taxa in bare and planted soil but the presence of plants modified their relative abundance. ^{13}C-enriched OTUs affiliated to *Arthrobacter*, unclassified *Sphingomonadaceae* and *Gammaproteobacteria* "PYR10d3" were present at a similar level in both conditions. Members of the *Actinobacteria* and *Sphingomonadaceae* are considered potent PAH-degraders in soil and sediments

[23,68,69,70]. Representatives of the *Arthrobacter* genus are able to degrade many organic pollutants [71]. Using DNA-SIP, some species were previously shown as the dominant phenanthrene degraders in soil supplemented with root exudates [14] and in activated sludge [26]. Interestingly, an *Arthrobacter oxydans* strain was isolated from the same soil used in the present study, for its ability to degrade phenanthrene [72]. The Pyr10d3 candidate order is a separate branch in *Gammaproteobacteria* first identified in a SIP experiment using ^{13}C-pyrene as substrate [29] and its abundance was increased considerably with the increase of petroleum-hydrocarbon contamination of a soil located close to petrochemical plant [73]. *Firmicutes* affiliated to *Paenibacillaceae* were only active in bare soil while in a previous study it was found as phenanthrene degraders when the soil was supplemented with root exudates [14]. *Paenibacillus* spp. were previously enriched from petroleum-hydrocarbon-contaminated sediment and salt marsh rhizosphere using either naphthalene or phenanthrene as the sole carbon source [74]. The greatest influence of ryegrass on active PHE-degraders was found for *Sphingomonas* and *Sphingobium*-related ^{13}C-enriched OTUs, which dominated in bare and planted soil, respectively. Sphingomonads, members of the family *Sphingomonadaceae* within the *Alphaproteobacteria*, utilize both substituted and unsubstituted mono- and poly-aromatic hydrocarbons up to 5-rings [27] and have been widely identified as phenanthrene degraders [24,75]. PAH-degrading sphingomonads are common Gram-negative, aerobic, chemoheterotroph bacteria adapted to oligotrophic environments [75]. They evolved original strategies to enhance PAH bioavailability, e.g. hydrophobic and negatively charged cell surface, production of a specific sphingoglycolipid, formation of biofilms due to sphingans exopolysaccharide production, presence of high-affinity uptake system, and chemotactic response towards PAH [75]. *Sphingomonas* spp. are commonly encountered in PAH-contaminated environments as phenanthrene degraders [11,22,23,68,75,76,77,78,79] and the amount of phenanthrene available in soils influences the diversity of *Sphingomonas* [18]. Similarly, representatives of *Sphingobium* can biodegrade environmental pollutants such as PAHs [80,81,82,83]. In bare soil, ^{13}C-enriched *Sphingomonas* OTUs coincided with a greater proportion of active *Alcaligenaceae* OTUs, while in rhizospheric soil *Sphingobium* OTUs were associated with a greater proportion of active unknown *Micrococcaceae*. *Alcaligenes* representatives were previously identified during creosote-contaminated soil bioremediation [84], and many studies showed PAH degradation by various *Alcaligenes* isolates [85,86,87]. *Micrococcaceae* are well-known PAH degraders [88,89] and their abundance was favoured in planted compared to bare aged-PAH contaminated soil [33].

To date, the impact of plant rhizosphere on the functional diversity was mostly assessed in pristine soils [90,91]. Our study is one of the first to highlight the differences in metagenomes of PAH-degrading bacteria from bulk and rhizospheric soil. We recovered enough ^{13}C-labeled DNA for direct shotgun metagenomic sequencing, overcoming the potential bias of multiple displacement amplification often used in DNA-SIP approaches [92]. The ^{13}C-enriched metagenomes from planted soil showed that ryegrass rhizosphere selected for an active population with specific functions compared to bare soil, i.e. a lower proportion of genes involved in aromatic compounds utilization together with a higher and diversified capability for carbohydrate degradation. This is reminiscent of the higher transcription of genes related to carbon and amino-acid uptake and utilization shown in the willow rhizosphere [93]. Moreover, the AromaDeg analysis confirmed the lower proportion of genes potentially involved in the first steps of aerobic degradation of aromatic compounds in planted soil metagenomes. Reconstruction of complete catabolic pathways (Figure 5) showed that several routes are used to mineralize phenanthrene both in bare and planted soil, since genes assigned to the o-phthalate/protocatechuate, gentisate and catechol ortho and meta-cleavage pathways were present. *Sphingomonadales* were the major taxa performing the first steps of phenanthrene degradation. They appear to degrade phenanthrene preferentially through lower meta-cleavage pathway, as it was shown for *Sphingobium chungbukense* [94]. These results suggest that autochthonous *Sphingomonadales* could have a critical role to initiate in-situ PAH remediation in historically polluted soils, by increasing PAH bioavailability and opening new substrate niches for other degraders. Our data further show that active PHE-degrading communities act as consortia, whereby the complete mineralization of phenanthrene is achieved through combined activity of taxonomically diverse co-occurring bacteria using various degradation pathways. This strategy might limit the competition for substrates between different degrading populations and overall increase PAH dissipation efficiency.

The dominant PHE-degraders *Sphingomonas* and *Sphingobium* OTUs were active both in bare and planted soils but in various proportions, leading to a lower phenanthrene degradation rate in the rhizosphere where *Sphingobium* dominated. Previous studies did not evidence a specificity of *Sphingomonas* and *Sphingobium* spp. for environments with low and high nutrient levels, respectively. For example, Vinas et al. [84] detected *Sphingomonas* in soil bioremediation treatments both with and without nutrient amendment. Recently, comparative genomics of *Novosphingobium* strains showed that phylogenetic relationships were less likely

to describe functional genotype similarity, in term of metabolic traits, than the habitat from which they were isolated [95]. Thus, catabolic differences among Sphingomonads appear strain-specific. Some Sphingomonad strains can simultaneously take up mixed substrates rather than being specialists in the degradation of aromatic compounds, because they can assimilate various mono-, di-, and polysaccharides [75,96]. The greater success of ^{13}C-enriched *Sphingobium* OTUs in planted soil, together with a larger diversity of CAZymes than the *Sphingomonas* metagenome from bare soil, suggests a similar behaviour. In the conditions tested, PHE-degrading *Sphingobium* representatives likely took advantage of labile carbon compounds from root exudates, outcompeting the less versatile PHE-degrading *Sphingomonas*.

Conclusion

In summary, this study identified the metabolically active phenanthrene degraders in an aged-polluted soil, and showed their taxonomic diversity among Alpha-, Beta- and Gammaproteobacteria, Actinobacteria and Firmicutes that could act as a consortium. Members of the Sphingomonadales were the dominant PHE-degraders identified through DNA-SIP, and the main actors of the first steps in the degradation pathways. Hence, they likely play a crucial role to initiate in-situ PAH remediation. Results further indicated that the presence of plants impacted the active PHE-degrading community and induced a slower PHE dissipation. In particular, plants induced a drastic shift in the taxonomic composition of PHE-degrading *Sphingomonadales*, favouring the growth of *Sphingobium* populations with a more diverse repertoire of carbohydrate-active enzymes potentially targeting plant root material, to the detriment of less versatile *Sphingomonas* representatives that prevailed in bare soil.

Acknowledgement.

This study was part of the RhizOrg project funded by the ANR (Agence Nationale de la Recherche, ANR-13-JSV7-0007_01 project allocate to A. Cébron). The authors thank Dr. S. Uroz (INRA Champenoux) for giving them access to the ultracentrifuge equipment, Dr. E. Morin (INRA Champenoux) for initial discussions on metagenome assembly, and the ABiMS platform (Roscoff) where metagenomic analyses were performed.

Conflict of interest

The authors declare that they have no conflict of interet.

References

1. Ghosal D, Ghosh S, Dutta TK, Ahn Y. Current state of knowledge in microbial degradation of polycyclic aromatic hydrocarbons (PAHs): a review. Front Microbiol. 2016; **7**:1369.
2. Khan S, Afzal M, Iqbal S, Khan QM. Plant–bacteria partnerships for the remediation of hydrocarbon contaminated soils. Chemosphere. 2013; **90**:1317-1332.
3. Doyle E, Muckian L, Hickey AM, Clipson N. Microbial PAH degradation. Adv Appl Microbiol. 2008; **65**:27-66.
4. Reilley KA, Banks MK, Schwab AP.Dissipation of polycyclic aromatic hydrocarbons in the rhizosphere. J Environ Qual. 1996; **25**:212-219.
5. Binet P, Portal JM, Leyval C. Dissipation of 3–6-ring polycyclic aromatic hydrocarbons in the rhizosphere of ryegrass. Soil Biol Biochem. 2000; **32**:2011-2017.
6. Chaudhry Q, Blom-Zandstra M, Gupta SK, Joner E. Utilising the synergy between plants and rhizosphere microorganisms to enhance breakdown of organic pollutants in the environment. Environ Sci Pollut Res. 2005; **12**:34-48.
7. El Amrani A, Dumas AS, Wick LY, Yergeau E, Berthomé R. "Omics" insights into PAH degradation toward improved green remediation biotechnologies. Environ Sci Technol. 2015; **49**:11281-11291.
8. Rentz JA, Alvarez PJ, Schnoor JL. Repression of Pseudomonas putida phenanthrene degrading activity by plant root extracts and exudates. Environ Microbiol. 2004; **6**:574-583.
9. Phillips LA, Greer CW, Farrell RE, Germida JJ. Plant root exudates impact the hydrocarbon degradation potential of a weathered-hydrocarbon contaminated soil. Appl Soil Ecol. 2012; **52**:56-64.
10. Berg G, Smalla K. Plant species and soil type cooperatively shape the structure and function of microbial communities in the rhizosphere. FEMS Microbiol Ecol. 2009; **68**:1-13.
11. Guo M, Gong Z, Miao R, Rookes J, Cahill D, Zhuang J. Microbial mechanisms controlling the rhizosphere effect of ryegrass on degradation of polycyclic aromatic hydrocarbons in an aged-contaminated agricultural soil. Soil Biol Biochem. 2017; **113**:130-142.

12. Thomas F, Cébron A. Short-term rhizosphere effect on available carbon sources phenanthrene degradation and active microbiome in an aged-contaminated industrial soil. Front Microbiol. 2016; **7**:92.
13. Olson PE, Castro A, Joern M, DuTeau NM, Pilon-Smits EA, Reardon KF, Comparison of plant families in a greenhouse phytoremediation study on an aged polycyclic aromatic hydrocarbon–contaminated soil. J Environ Qual. 2007; **36**:1461-1469.
14. Cébron A, Louvel B, Faure P, France‐Lanord C, Chen Y, Murrell JC, Leyval C. Root exudates modify bacterial diversity of phenanthrene degraders in PAH‐polluted soil but not phenanthrene degradation rates. Environ Microbiol. 2011; **13**:722-736.
15. Sul WJ, Park J, Quensen JF, Rodrigues JL, Seliger L, Tsoi TV et al. DNA-stable isotope probing integrated with metagenomics for retrieval of biphenyl dioxygenase genes from polychlorinated biphenyl-contaminated river sediment. Appl Environ Microbiol. 2009; **75**:5501-5506.
16. Kim SJ, Park SJ, Cha IT, Min D, Kim JS, Chung WH et al. Metabolic versatility of toluene‐degrading iron‐reducing bacteria in tidal flat sediment characterized by stable isotope probing‐based metagenomic analysis. Environ Microbiol. 2014; **16**:189-204.
17. Jeon CO, Park W, Padmanabhan P, DeRito C, Snape JR, Madsen EL. Discovery of a bacterium with distinctive dioxygenase that is responsible for in situ biodegradation in contaminated sediment. PNAS. 2003; **100**:13591-13596.
18. Singleton DR, Powell SN, Sangaiah R, Gold A, Ball LM, Aitken MD. Stable-isotope probing of bacteria capable of degrading salicylate naphthalene or phenanthrene in a bioreactor treating contaminated soil. Appl Environ Microbiol. 2005; **71**:1202-1209.
19. Padmanabhan P, Padmanabhan S, DeRito C, Gray A, Gannon D, Snape JR et al. Respiration of 13C-labeled substrates added to soil in the field and subsequent 16S rRNA gene analysis of 13C-labeled soil DNA. Appl Environ Microbiol. 2003; **69**:1614-1622.
20. Uhlik O, Wald J, Strejcek M, Musilova L, Ridl J, Hroudova M et al. Identification of bacteria utilizing biphenyl benzoate and naphthalene in long-term contaminated soil. PloS One. 2012; **7**:e40653.
21. Jiang L, Song M, Luo C, Zhang D, Zhang G. Novel phenanthrene-degrading bacteria identified by DNA-stable isotope probing. PloS One. 2015; **10**:e0130846.

569 22. Martin F, Torelli S, Le Paslier D, Barbance A, Martin-Laurent F, Bru D et al.
570 Betaproteobacteria dominance and diversity shifts in the bacterial community of a PAH-
571 contaminated soil exposed to phenanthrene. Environ Pollut. 2012; **162**:345-353.
572 23. Regonne RK, Martin F, Mbawala A, Ngassoum MB, Jouanneau Y. Identification of soil
573 bacteria able to degrade phenanthrene bound to a hydrophobic sorbent in situ. Environ
574 Pollut. 2013; **180**:145-151.
575 24. Song M, Jiang L, Zhang D, Luo C, Wang Y, Yu Z, Zhang G. Bacteria capable of
576 degrading anthracene phenanthrene and fluoranthene as revealed by DNA based stable-
577 isotope probing in a forest soil. J Hazard Mat. 2016; **308**:50-57.
578 25. Crampon M, Cébron A, Portet-Koltalo F, Uroz S, Le Derf F, Bodilis J. Low effect of
579 phenanthrene bioaccessibility on its biodegradation in diffusely contaminated soil. Environ
580 Pollut. 2017; **225**:663-673.
581 26. Li J, Zhang D, Song M, Jiang L, Wang Y, Luo C, Zhang G. Novel bacteria capable of
582 degrading phenanthrene in activated sludge revealed by stable-isotope probing coupled
583 with high-throughput sequencing. Biodeg. 2017; **28**:423-436.
584 27. Jones MD, Crandell DW, Singleton DR, Aitken MD. Stable isotope probing of the
585 polycyclic aromatic hydrocarbon degrading bacterial guild in a contaminated soil. Environ
586 Microbiol. 2011; **13**:2623-2632.
587 28. Zhang S, Wang Q, Xie S. Stable isotope probing identifies anthracene degraders under
588 methanogenic conditions. Biodeg. 2012; **23**:221-230.
589 29. Singleton DR, Sangaiah R, Gold A, Ball LM, Aitken MD. Identification and
590 quantification of uncultivated Proteobacteria associated with pyrene degradation in a
591 bioreactor treating PAH contaminated soil. Environ Microbiol. 2006; **8**:1736-1745.
592 30. Jones MD, Singleton DR, Carstensen DP, Powell SN, Swanson JS, Pfaender FK, Aitken
593 MD. Effect of incubation conditions on the enrichment of pyrene-degrading bacteria
594 identified by stable-isotope probing in an aged PAH-contaminated soil. Microb Ecol. 2008;
595 **56**:341-349.
596 31. Song M, Luo C, Jiang L, Zhang D, Wang Y, Zhang G. Identification of benzo [a] pyrene
597 (BaP)-metabolizing bacteria in forest soils using DNA-based stable-isotope probing. Appl
598 Environ Microbiol. 2015; **81**:7368-7376.
599 32. el Zahar Haichar F, Marol C, Berge O, Rangel-Castro JI, Prosser JI, Balesdent J,
600 Achouak W. Plant host habitat and root exudates shape soil bacterial community structure.
601 ISME J. 2008; **2**:1221.

602 33. Cébron A, Beguiristain T, Faure P, Norini M-P, Masfaraud J-F, Leyval C. Influence of
603 vegetation on the in situ bacterial community and polycyclic aromatic hydrocarbon (PAH)
604 degraders in aged PAH-contaminated or thermal-desorption-treated soil. Appl Environ
605 Microbiol. 2009; **75**: 6322–30.
606 34. Biache C, Mansuy-Huault L, Faure P, Munier-Lamy C, Leyval C. Effects of thermal
607 desorption on the composition of two coking plant soils: Impact on solvent extractable
608 organic compounds and metal bioavailability. Environ Pollut. 2008; **156**: 671-677.
609 35. Biache C, Ouali S, Cébron A, Lorgeoux C, Colombano S, Faure P. Bioremediation of
610 PAH-contamined soils: consequences on formation and degradation of polar-polycyclic
611 aromatic compounds and microbial community abundance. J Hazard Mat. 2017; **329**:1-10.
612 36. Dunford E, Neufeld JD. DNA stable-isotope probing (DNA-SIP). J Vis Exp. 2010; **2**: 1-
613 6.
614 37. Felske A, Akkermans ADL, De Vos WM. Quantification of 16S rRNAs in complex
615 bacterial communities by multiple competitive reverse transcription-PCR in temperature
616 gradient gel electrophoresis fingerprints. Appl Environ Microbiol. 1998; **64**: 4581-4587.
617 38. Baker GC, Smith JJ, Cowan DA. Review and re-analysis of domain-specific 16S primers.
618 J Microbiol Meth. 2003; **55**:541-555.
619 39. Smit E, Smit E, Leeflang P, Leeflang P, Glandorf B, Glandorf B et al. Analysis of fungal
620 diversity in the wheat rhizosphere by sequencing of cloned PCR-Amplied genes encoding
621 18S rRNA and temperature gradient gel electrophoresis. Society. 1999; **65**: 2614–2621.
622 40. Vainio EJ, Hantula J. Direct analysis of wood-inhabiting fungi using denaturing gradient
623 gel electrophoresis of amplified ribosomal DNA. Mycol Res. 2000; **104**: 927–936.
624 41. Cébron A, Norini M-P, Beguiristain T, Leyval C. Real-Time PCR quantification of PAH-
625 ring hydroxylating dioxygenase (PAH-RHDα) genes from Gram positive and Gram
626 negative bacteria in soil and sediment samples. J Microbiol Methods. 2008; **73**: 148–59
627 42. Kozich JJ, Westcott SL, Baxter NT, Highlander SK, Schloss PD. Development of a dual-
628 index sequencing strategy and curation pipeline for analyzing amplicon sequence data on
629 the MiSeq Illumina sequencing platform. Appl Environ Microbiol. 2013; **79**: 5112–20.
630 43. Masella AP, Bartram AK, Truszkowski JM, Brown DG, Neufeld JD. PANDAseq:
631 paired-end assembler for Illumina sequences. BMC Bioinformatics. 2012; **13**: 31.
632 44. Caporaso JG, Kuczynski J, Stombaugh J, Bittinger K, Bushman FD, Costello EK, et al.
633 QIIME allows analysis of high-throughput community sequencing data. Nat Methods.
634 2010; **7**: 335–6.

45. Edgar RC. Search and clustering orders of magnitude faster than BLAST. Bioinformatics. 2010; **26**: 2460–1.
46. Edgar RC, Haas BJ, Clemente JC, Quince C, Knight R. UCHIME improves sensitivity and speed of chimera detection. Bioinformatics. 2011; **27**: 2194–2200.
47. Wang Q, Garrity GM, Tiedje JM, Cole JR. Naive Bayesian classifier for rapid assignment of rRNA sequences into the new bacterial taxonomy. Appl Environ Microbiol. 2007; **73**: 5261–7.
48. McDonald D, Price MN, Goodrich J, Nawrocki EP, DeSantis TZ, Probst A, et al. An improved Greengenes taxonomy with explicit ranks for ecological and evolutionary analyses of bacteria and archaea. ISME J. 2012; **6**: 610–8.
49. R Core TeamR: A Language and Environment for Statistical Computing. 2013. Vienna, Austria.
50. Bolger AM, Lohse M, Usadel B. Trimmomatic: A flexible trimmer for Illumina sequence data. Bioinformatics. 2014; **30**: 2114–2120.
51. Meyer F, Paarmann D, D'Souza M, etal. The metagenomics RAST server—a public resource for the automatic phylo- genetic and functional analysis of metagenomes. BMC Bioinformatics. 2008; **9**: 386.
52. Bankevich A, Nurk S, Antipov D, Gurevich AA, Dvorkin M, Kulikov AS, et al. SPAdes: A New Genome Assembly Algorithm and Its Applications to Single-Cell Sequencing. J Comput Biol. 2012; **19**: 455–477.
53. Patil KR, Roune L, McHardy AC. The phyloPythiaS web server for taxonomic assignment of metagenome sequences. PLoS One. 2012; **7:** e38581..
54. Seemann T. Prokka: rapid prokaryotic genome annotation. Bioinformatics. 2014. **30:** 2068-2069.
55. Duarte M Jauregui R Vilchez-Vargas R Junca H Pieper DH. AromaDeg a novel database for phylogenomics of aerobic bacterial degradation of aromatics. Database. 2014; 1–12.
56. Katoh K, Rozewicki J, Yamada KD. MAFFT online service: multiple sequence alignment interactive sequence choice and visualization. Brief Bioinform. 2017; 1–7.
57. Waterhouse AM, Procter JB, Martin DMA, Clamp M, Barton GJ. Jalview Version 2-A multiple sequence alignment editor and analysis workbench. Bioinformatics 2009; **25**: 1189–1191.
58. Tamura K, Stecher G, Peterson D, Filipski A, Kumar S. MEGA6: Molecular evolutionary genetics analysis version 6.0. Mol Biol Evol. 2013; **30**: 2725–2729.

668 59. Yin Y, Mao X, Yang J, Chen X, Mao F, Xu Y. DbCAN: A web resource for automated
669 carbohydrate-active enzyme annotation. Nucleic Acids Res. 2012; **40**: 445–451.
670 60. Kanehisa M, Sato Y, Morishima K. BlastKOALA and GhostKOALA: KEGG tools for
671 functional characterization of genome and metagenome sequences. J Mol Biol. 2016; **428**:
672 726–731.
673 61. Tabata M, Ohtsubo Y, Ohhata S, Tsuda M, Nagata Y. Complete genome sequence of the
674 γ-hexachlorocyclohexane-degrading bacterium Sphingomonas spstrain MM-1. Genome
675 Announcements. 2013; **1**:e00247-13.
676 62. Zipper C, Nickel K, Angst W, Kohler HP. Complete microbial degradation of both
677 enantiomers of the chiral herbicide mecoprop [(RS)-2-(4-chloro-2-methylphenoxy)
678 propionic acid] in an enantioselective manner by Sphingomonas herbicidovorans sp. nov.
679 Appl Environ Microbiol. 1996; **62**: 4318-4322.
680 63. Tabata M, Ohhata S, Nikawadori Y, Sato , TKishida K, Ohtsubo Y et al. Complete
681 genome sequence of a γ-hexachlorocyclohexane-degrading bacterium Sphingobium
682 spstrain MI1205. Genome Announcements. 2016; **4**:e00246-16.
683 64. Rezek J, Mackova M, Zadrazil F, Macek T. The effect of ryegrass (Lolium perenne) on
684 decrease of PAH content in long term contaminated soil. Chemosphere. 2008; **70:**1603-
685 1608.
686 65. Chaillan F, Chaineau CH, Point V, Saliot A, Oudot J. Factors inhibiting bioremediation
687 of soil contaminated with weathered oils and drill cuttings. Environ Pollut. 2006; **144:**255-
688 265.
689 66. Carmichael LM, Pfaender FK. The effect of inorganic and organic supplements on the
690 microbial degradation of phenanthrene and pyrene in soils. Biodeg. 1997; **8**:1-13.
691 67. Chaineau CH, Rougeux G, Yepremian C, Oudot J. Effects of nutrient concentration on
692 the biodegradation of crude oil and associated microbial populations in the soil. Soil Biol
693 Biochem. 2005; **37:**1490-1497.
694 68. Leys NM, Ryngaert A, Bastiaens L, Verstraete W, Top EM, Springael D. Occurrence and
695 phylogenetic diversity of *Sphingomonas* strains in soils contaminated with polycyclic
696 aromatic hydrocarbons. Appl Environ Microbiol. 2004; **70:**1944-1955.
697 69. Leys NM, Bastiaens L, Verstraete W, Springael D. Influence of the
698 carbon/nitrogen/phosphorus ratio on polycyclic aromatic hydrocarbon degradation by
699 Mycobacterium and Sphingomonas in soil. Appl Microbiol Biotechnol. 2005; **66:**726-736.

70. Alonso-Gutiérrez J, Figueras A, Albaigés J, Jiménez N, Vinas M, Solanas AM, Novoa B. Bacterial communities from shoreline environments (Costa da Morte Northwestern Spain) affected by the Prestige oil spill. Appl Environ Microbiol. 2009; 75:3407-3418.
71. Leigh MB, Pellizari VH, Uhlík O, Sutka R, Rodrigues J, Ostrom NE et al. Biphenyl-utilizing bacteria and their functional genes in a pine root zone contaminated with polychlorinated biphenyls (PCBs). ISME J. 2007; **1:**134.
72. Thion C, Cébron A, Beguiristain T, Leyval C. PAH biotransformation and sorption by Fusarium solani and Arthrobacter oxydans isolated from a polluted soil in axenic cultures and mixed co-cultures. Int Biodeter Biodeg. 2012; **68:**28-35.
73. Tardif S, Yergeau É, Tremblay J, Legendre P, Whyte LG, Greer CW. The willow microbiome is influenced by soil petroleum-hydrocarbon concentration with plant compartment-specific effects. Front Microbiol. 2016; **7:**1363.
74. Daane LL, Harjono I, Barns SM, Launen LA, Palleron NJ, Häggblom MM. PAH-degradation by Paenibacillus sppand description of Paenibacillus naphthalenovorans spnova naphthalene-degrading bacterium from the rhizosphere of salt marsh plants. Int J Syst Evol Microbiol. 2002; **52:**131-139.
75. Waigi MG, Kang F, Goikavi C, Ling W, Gao Y. Phenanthrene biodegradation by sphingomonads and its application in the contaminated soils and sediments: a review. Int Biodeter Biodeg. 2015; **104:**333-349.
76. Daane LL, Harjono I, Zylstra GJ, Häggblom MM. Isolation and characterization of polycyclic aromatic hydrocarbon-degrading bacteria associated with the rhizosphere of salt marsh plants. Appl Environ Microbiol. 2001; **67:**2683-2691.
77. Johnsen AR, Winding A, Karlson U, Roslev P. Linking of microorganisms to phenanthrene metabolism in soil by analysis of 13C-labeled cell lipids. Appl Environ Microbiol. 2002; **68:**6106-6113.
78. Meyer S, Moser R, Neef A, Stahl U, Kämpfer P. Differential detection of key enzymes of polyaromatic-hydrocarbon-degrading bacteria using PCR and gene probes. Microbiol. 1999; **145:**1731-1741.
79. Ding GC, Heuer H, Smalla K. Dynamics of bacterial communities in two unpolluted soils after spiking with phenanthrene: soil type specific and common responders. Front Microbiol. 2012; **3:**290.
80. Kanaly RA, Harayama S. Biodegradation of high-molecular-weight polycyclic aromatic hydrocarbons by bacteria. J Bacteriol. 2000; **182:**2059-2067.

733 81. Kanaly RA, Harayama S. Advances in the field of high‐molecular‐weight polycyclic
734 aromatic hydrocarbon biodegradation by bacteria. Microb Biotechnol. 2010; **3:**136-164.
735 82. Stolz A. Molecular characteristics of xenobiotic-degrading sphingomonads. Appl
736 Microbiol Biotechnol. 2009; **81:**793-811.
737 83. Maeda AH, Kunihiro M, Ozeki Y, Nogi Y, Kanaly RA. Sphingobium barthaii spnova
738 high molecular weight polycyclic aromatic hydrocarbon-degrading bacterium isolated
739 from cattle pasture soil. Int J Syst Evolut Microbiol. 2015; **65:**2919-2924.
740 84. Vinas M, Sabaté J, Espuny MJ, Solanas AM. Bacterial community dynamics and
741 polycyclic aromatic hydrocarbon degradation during bioremediation of heavily creosote-
742 contaminated soil. Appl Environ Microbiol. 2005; **71:**7008-7018.
743 85. Weissenfels WD, Beyer M, Klein J. Degradation of phenanthrene fluorene and
744 fluoranthene by pure bacterial cultures. Appl Microbiol Biotechnol. 1990; **32:**479-484.
745 86. Lal B, Khanna S. Degradation of crude oil by *Acinetobacter calcoaceticus* and
746 *Alcaligenes odorans*. J Appl Bacteriol. 1996; **81:**355-362.
747 87. Samanta SK, Singh OV, Jain RK. Polycyclic aromatic hydrocarbons: environmental
748 pollution and bioremediation. TRENDS Biotechnol. 2002; **20:**243-248.
749 88. Kästner M, Breuer-Jammali M, Mahro B. Enumeration and characterization of the soil
750 microflora from hydrocarbon-contaminated soil sites able to mineralize polycyclic
751 aromatic hydrocarbons (PAH). Appl Microbiol Biotechnol. 1994; **41:**267-273.
752 89. Margesin R, Moertelmaier C, Mair J. Low-temperature biodegradation of petroleum
753 hydrocarbons (n-alkanes phenol anthracene pyrene) by four actinobacterial strains. Int
754 Biodeter Biodeg. 2013; **84:**185-191.
755 90. Uroz S, Ioannidis P, Lengelle J, Cébron A, Morin E, Buée M, Martin F. Functional
756 assays and metagenomic analyses reveals differences between the microbial communities
757 inhabiting the soil horizons of a Norway spruce plantation. PLoS One. 2013; **8:**e55929.
758 91. Mendes LW, Kuramae EE, Navarrete AA, Van Veen JA, Tsai SM. Taxonomical and
759 functional microbial community selection in soybean rhizosphere. ISME J. 2014; **8:**1577.
760 92. Verastegui Y, Cheng J, Engel K, Kolczynski D, Mortimer S, Lavigne J et al.
761 Multisubstrate isotope labeling and metagenomic analysis of active soil bacterial
762 communities. MBio. 2014; **5:**e01157-14.
763 93. Yergeau E, Sanschagrin S, Maynard C, St-Arnaud M, Greer CW. Microbial expression
764 profiles in the rhizosphere of willows depend on soil contamination. ISME J. 2014; **8:**344.

765 94. Lee SY, Sekhon SS, Ban YH, Ahn JY, Ko JH, Lee L, Kim SY, Kim YC, Kim YH.
766 Proteomic analysis of polycyclic aromatic hydrocarbons (PAHs) degradation and
767 detoxification in Sphingobium chungbukense. J Microbiol Biotechnol. 2016; **26:**1943–
768 1950
769 95. Kumar R, Verma H, Haider S, Bajaj A, Sood U, Ponnusamy K et al. Comparative
770 genomic analysis reveals habitat-specific genes and regulatory hubs within the genus
771 Novosphingobium. MSystems. 2017; **2:**e00020-17.
772 96. Tao XQ, Lu GN, Dang Z, Yang C, Yi XY. A phenanthrene-degrading strain
773 Sphingomonas spGY2B isolated from contaminated soils. Process Biochem. 2007; **42:**401-
774 408.
775
776

Tables

Table 1. Proportion of ^{13}C remaining (after 10 days incubation, D10) compared to the amount added at D0 in total soil, soil residue, dichloromethane extract measured using AE-IRMS and of ^{13}C-phenanthrene in dichloromethane extract measured using GC-MS.

Table 2: Normalized prevalence of genes encoding enzymes for aerobic bacterial degradation of aromatics in ^{13}C-labeled metagenomes, relative to *recA*. Values are mean ± s.e.m (n=3), based on features identified using AromaDeg on assembled contigs. The difference between bare and planted condition was tested using Welch's test.

Table 3. Detection of genes encoding putative carbohydrate active enzymes (CE: carbohydrate esterase; GH: glycoside hydrolase; PL: polysaccharide lyase) in ^{13}C-enriched metagenomes from *Sphingomonas* and *Sphingobium* in bare and planted SIP incubations, respectively. Counts are given for the three independent replicates.

Figure Legends

Figure 1. A. Taxonomic profiling of heavy DNA from ^{12}C-controls and ^{13}C-SIP incubations, in bare or planted microcosms. Values are means of three independent microcosms. **B.** Abundance of taxonomic groups significantly enriched in heavy DNA fractions from ^{13}C-SIP conditions compared to the ^{12}C-controls in bare (white) and planted conditions (grey). Values are depicted on a log-scale and are mean ± s.e.m.(n=3). Values in brackets beside each bar represent the number of OTUs.

Figure 2. Functional analysis of shotgun metagenomic paired-end reads from bare and planted ^{13}C-SIP experiments (mean ± SD, n=3) based on subsystem categories in MG-RAST. Relative abundance of the 28 functional categories (A), the 12 carbohydrate metabolism categories (B) and the 4 categories concerning the metabolism of aromatic compounds (C), with some sub-categories shown when significant differences were obtained between bare and planted conditions. Relative abundances were expressed based on the total

number of hits provided by MG-RAST analysis, i.e. 5 394 642, 5 631 202 and 4 264 598 for triplicates of bare soil metagenomes, and 4 060 525, 5 619 868 and 4 759 581 for triplicates of planted soil metagenomes. Asterisks indicate statistically significant differences (q-values < 0.05 after Benjamini-Hochberg correction) between bare and planted conditions.

Figure 3. Maximum-likelihood (ML) phylogenetic reconstructions of dioxygenases (alpha-subunit of Rieske non-heme iron oxygenases) of the biphenyl/naphthalene family from **A)** *Proteobacteria* (AromaDeg Clusters XXIV and XXVI) and **B)** *Actinobacteria* (Clusters I, II and V), identified in ^{13}C-enriched assembled metagenomes from bare (orange; NPA, NPB, NPC) and planted (green; RGA, RGB, RGC) SIP microcosms. Sequences from reference strains are included with their accession number and experimentally validated substrate (Pht: phthalate; Non: unknown; Paa: polycyclic aromatic hydrocarbons (*Actinobacteria*); Pap: polycyclic aromatic hydrocarbons (*Proteobacteria*); Nah: naphthalene; Bph: biphenyl; Phn: phenanthrene; DbtA: dibenzothiophene; Dnt: dinitrotoluene). The LG+G+I (G=1.62, I=0.02) and LG+G (G=0.57) substitution models were respectively used for A) and B) after evaluating the best model in MEGA6. ML bootstrap support (100 re-samplings) are given. Bars represent fraction of sequence divergence.

Figure 4. Maximum-likelihood (ML) phylogenetic reconstruction of extradiol dioxygenases of the vicinal oxygen chelate family (EXDO I) from AromaDeg Cluster XII, identified in ^{13}C-enriched assembled metagenomes from bare (orange; NPA, NPB, NPC) and planted (green; RGA, RGB, RGC) SIP microcosms. Sequences from reference strains are included with their accession number and experimentally validated substrate (Dhb: 2,3-dihydroxybiphenyl; Dhn: Dihydroxynaphthalene; Dhp: 2,3-Dihydroxybiphenyl and dihydroxylated polycyclic aromatic hydrocarbons (probably dihydroxyphenanthrene); Dhe: 2,3-Dihydroxy-1-ethylbenzene; Thn: 1,2-Dihydroxy-5,6,7, 8-tetrahydronaphthalene; DbtC, 2,3-Dihydroxybiphenyl, probably dihydroxydibenzothiophene and dihydroxylated polycyclic aromatic hydrocarbons; Non: unknown). The LG+G+I substitution model was used (G=1.09, I=0.09) after evaluating the best model in MEGA6. ML bootstrap support (100 re-samplings) are given. The bar represents fraction of sequence divergence.

Figure 5. Reconstruction of phenanthrene metabolic pathways. Red arrows represent genes described in Figures 3 - 4 and enzyme families described in AromaDeg. Black arrows are genes found in both metagenomes using GhostKOALA with the reaction identifiers with

844 enzyme names, EC number, gene names and identification numbers of each reaction. The
845 number of genes identified in the two conditions is added in orange (bare soil, NP) and green
846 (planted soil, RG) above bar graphs with the taxonomic affiliation of identified genes. Note
847 that 32.1% (114 211 / 355 456) and 29.8% (225 994 / 758 006) of the entries could be
848 assigned to known functions for bare and planted soils, respectively.
849
850
851

Table 1. Proportion of ^{13}C remaining (after 10 days incubation, D10) compared to the amount added at D0 in total soil, soil residue, dichloromethane extract measured using AE-IRMS and of ^{13}C-phenanthrene in dichloromethane extract measured using GC-MS.

	proportion of ^{13}C remaining compared to amount added at D0 (%)[a]			
	AE-IRMS			GC-MS
	total soil	soil residue	DCM extract	DCM extract
D0	100.0 ± 6.4	3.5 ± 0.7	100.0 ± 7.6	100.0 ± 9.2
Bare D10	97.8 ± 6.7	13.0 ± 0.7	79.9 ± 10.7	74.3 ± 1.9
Planted D10	99.1 ± 2.3	5.8 ± 0.2	90.5 ± 1.2	87.9 ± 0.9

DCM: dichloromethane, [a]values are mean ± s.e.m. (n=3)

Table 2: Normalized prevalence of genes encoding enzymes for aerobic bacterial degradation of aromatics in ^{13}C-labeled metagenomes, relative to *recA*. Values are mean ± s.e.m (n=3), based on features identified using AromaDeg on assembled contigs. The difference between bare and planted condition was tested using Welch's test.

Enzyme class	Prevalence relative to *recA*		
	Bare	**Planted**	**pval**
Benzoate oxygenase	6.6±0.9	2.0±0.2	0.007
Biphenyl/naphthalene oxygenase	5.2±0.9	1.8±0.1	0.018
Extradiol dioxygenase, vicinal oxygen chelate	6.1±1.2	2.6±0.1	0.039
Gentisate oxygenase	2.3±0.7	1.2±0.2	0.171
Homoprotocatechuate oxygenase	1.0±0.0	0.5±0.0	0.001
Protocatechuate oxygenase	2.0±0.9	1.0±0.1	0.304
Phthalate oxygenase	4.0±1.5	1.2±0.0	0.138
Salicylate oxygenase	7.7±1.1	2.5±0.2	0.011

Table 3. Detection of genes encoding putative carbohydrate active enzymes (CE: carbohydrate esterase; GH: glycoside hydrolase; PL: polysaccharide lyase) in ^{13}C-enriched metagenomes from *Sphingomonas* and *Sphingobium* in bare and planted SIP incubations, respectively. Counts are given for the three independent replicates.

CAZY family	Counts based on dbcan annotation in ^{13}C-enriched metagenomes						Example of known activities in family
	Sphingomonas in bare soil			***Sphingobium*** in planted soil			
CE1	6	6	5	4	4	4	xylanase
CE14	0	0	0	1	1	1	diacetylchitobiose deacetylase
CE3	2	2	0	2	2	2	acetyl xylan esterase
CE4	4	4	3	1	1	1	chitooligosaccharide deacetylase, peptidoglycan N-acetylglucosamine deacetylase, acetyl xylan esterase
CE6	0	0	0	1	1	1	acetyl xylan esterase
CE7	0	0	0	1	1	1	acetyl xylan esterase
GH1	3	4	3	0	0	0	β-glucosidases, β-galactosidases
GH10	0	0	0	1	1	1	endo-xylanase
GH102	2	1	1	1	1	1	peptidoglycan lytic transglycosylase
GH103	2	2	1	1	1	1	peptidoglycan lytic transglycosylase
GH108	1	1	1	1	1	1	N-acetylmuramidase
GH109	2	2	2	2	2	1	α-N-acetylgalactosaminidase
GH115	0	0	0	2	2	2	xylan α-1,2-glucuronidase
GH13	1	1	1	3	3	3	α-glucosidase
GH130	2	2	2	0	0	0	β-1,4-mannosylglucose phosphorylase
GH136	0	0	0	1	1	1	lacto-N-biosidase
GH15	1	1	1	1	1	1	exolytic glucoamylase
GH16	0	0	0	2	2	2	wide variety of activities on β-1,4 or β-1,3 glycosidic bonds
GH23	5	7	6	5	4	4	peptidoglycan lyases
GH24	2	0	1	0	0	0	lysozyme
GH25	0	0	0	1	1	1	lysozyme
GH28	1	1	1	0	0	0	polygalacturonases
GH3	1	1	1	4	4	4	β-D-glucosidases, α-L-arabinofuranosidases, β-D-xylopyranosidases, *N*-acetyl-β-D-glucosaminidases
GH43_12	0	0	0	1	1	1	endo-β-1,4-xylanase / α-L-arabinofuranosidase
GH5	4	4	0	0	0	0	endoglucanase, endomannanase
GH65	0	0	0	1	1	1	maltose phosphorylase, trehalose phosphorylase, kojibiose phosphorylase, and trehalose 6-phosphate phosphorylase
GH67	0	0	0	1	1	1	xylan α-1,2-glucuronidase
GH73	0	0	1	0	0	0	lysozyme
GH74	2	2	1	0	0	0	xyloglucanase
GH76	1	1	0	0	0	0	α-1,6-mannanase
PL1_2	0	0	0	2	2	2	pectin/pectate lyase
PL12	1	1	1	1	1	1	heparin-sulfate lyase
PL15_2	0	0	0	1	1	1	alginate lyase
PL22	2	2	2	5	5	5	oligogalacturonate lyase
PL6	2	2	2	1	1	1	alginate lyase, chondroitinase B
total families	21	20	19	27	27	27	
total CAZymes	47	47	36	48	47	46	

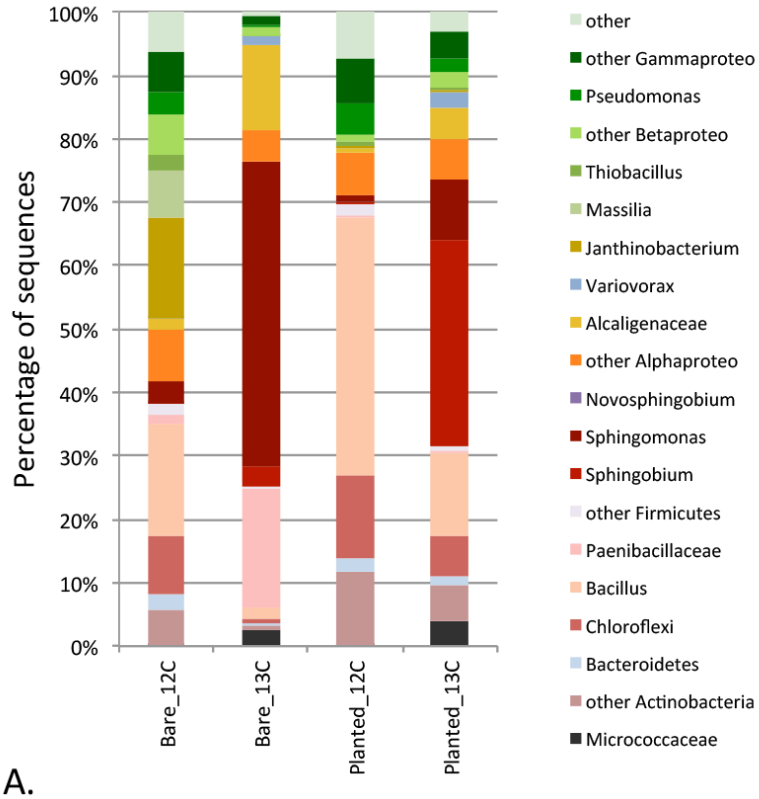
100%
90%
80%
70%
60%
50%
40%
30%
20%
10%
0%
Percentage of sequences
Bare_12C
Bare_13C
Planted_12C
Planted_13C
other
other Gammaproteo
Pseudomonas
other Betaproteo
Thiobacillus
Massilia
Janthinobacterium
Variovorax
Alcaligenaceae
other Alphaproteo
Novosphingobium
Sphingomonas
Sphingobium
other Firmicutes
Paenibacillaceae
Bacillus
Chloroflexi
Bacteroidetes
other Actinobacteria
Micrococcaceae

A.

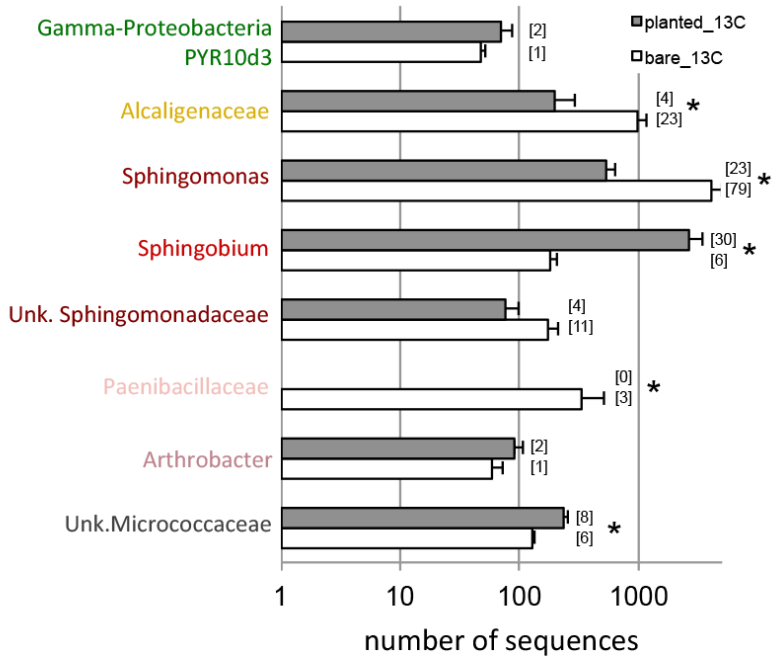
Gamma-Proteobacteria PYR10d3
Alcaligenaceae
Sphingomonas
Sphingobium
Unk. Sphingomonadaceae
Paenibacillaceae
Arthrobacter
Unk.Micrococcaceae
planted_13C
bare_13C
[2]
[1]
[4]
[23]
*
[23]
[79]
*
[30]
[6]
*
[4]
[11]
[0]
[3]
*
[2]
[1]
[8]
[6]
*
1
10
100
1000
number of sequences

B.

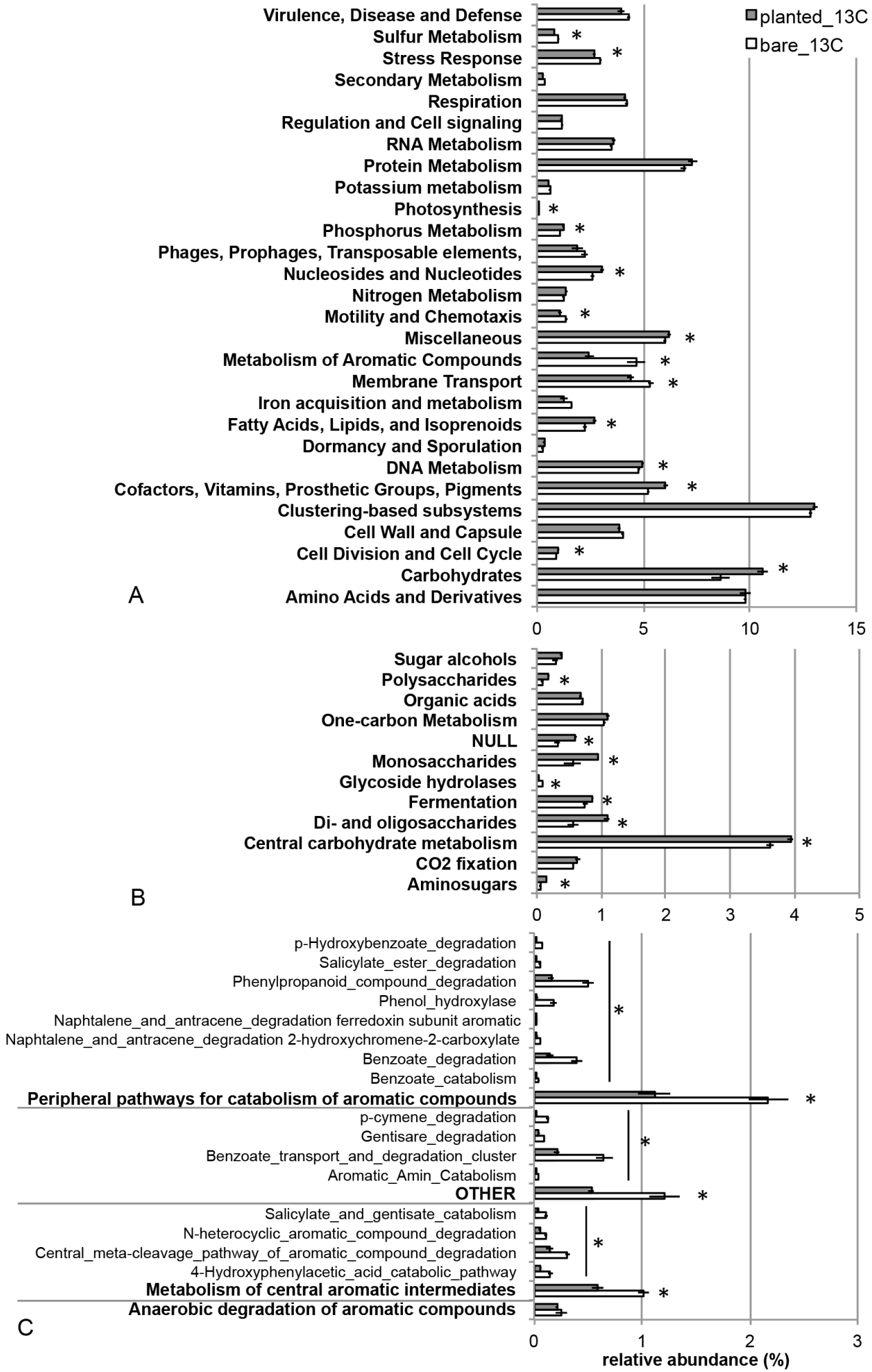
planted_13C
bare_13C
Virulence, Disease and Defense
Sulfur Metabolism
Stress Response
Secondary Metabolism
Respiration
Regulation and Cell signaling
RNA Metabolism
Protein Metabolism
Potassium metabolism
Photosynthesis
Phosphorus Metabolism
Phages, Prophages, Transposable elements,
Nucleosides and Nucleotides
Nitrogen Metabolism
Motility and Chemotaxis
Miscellaneous
Metabolism of Aromatic Compounds
Membrane Transport
Iron acquisition and metabolism
Fatty Acids, Lipids, and Isoprenoids
Dormancy and Sporulation
DNA Metabolism
Cofactors, Vitamins, Prosthetic Groups, Pigments
Clustering-based subsystems
Cell Wall and Capsule
Cell Division and Cell Cycle
Carbohydrates
Amino Acids and Derivatives
A
0
5
10
15
Sugar alcohols
Polysaccharides
Organic acids
One-carbon Metabolism
NULL
Monosaccharides
Glycoside hydrolases
Fermentation
Di- and oligosaccharides
Central carbohydrate metabolism
CO2 fixation
Aminosugars
B
0
1
2
3
4
5
p-Hydroxybenzoate_degradation
Salicylate_ester_degradation
Phenylpropanoid_compound_degradation
Phenol_hydroxylase
Naphtalene_and_antracene_degradation ferredoxin subunit aromatic
Naphtalene_and_antracene_degradation 2-hydroxychromene-2-carboxylate
Benzoate_degradation
Benzoate_catabolism
Peripheral pathways for catabolism of aromatic compounds
p-cymene_degradation
Gentisare_degradation
Benzoate_transport_and_degradation_cluster
Aromatic_Amin_Catabolism
OTHER
Salicylate_and_gentisate_catabolism
N-heterocyclic_aromatic_compound_degradation
Central_meta-cleavage_pathway_of_aromatic_compound_degradation
4-Hydroxyphenylacetic_acid_catabolic_pathway
Metabolism of central aromatic intermediates
Anaerobic degradation of aromatic compounds
C
0
1
2
3
relative abundance (%)

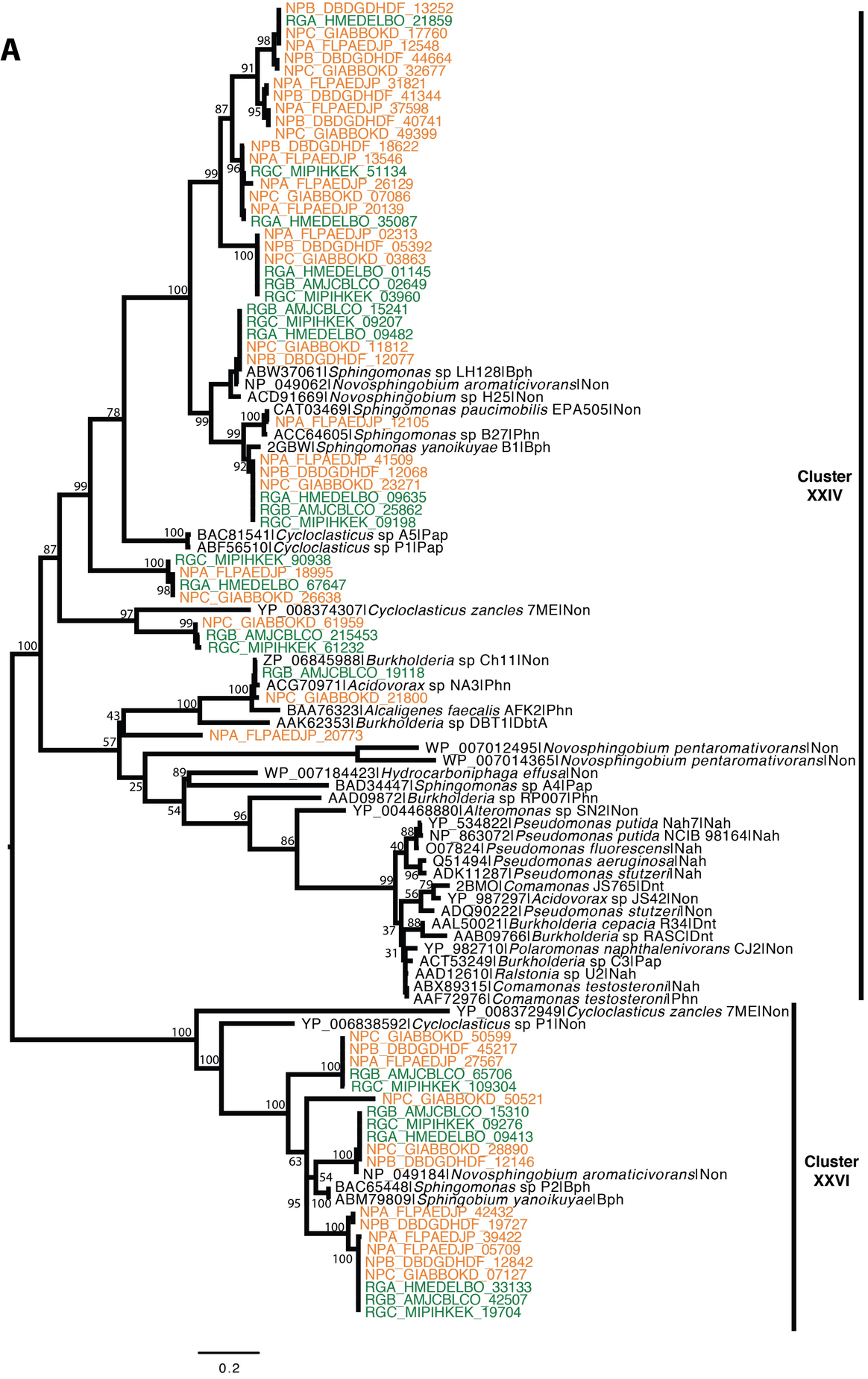
A
NPB_DBDGDHDF_13252
RGA_HMEDELBO_21859
NPC_GIABBOKD_17760
NPA_FLPAEDJP_12548
NPB_DBDGDHDF_44664
NPC_GIABBOKD_32677
NPA_FLPAEDJP_31821
NPB_DBDGDHDF_41344
NPA_FLPAEDJP_37598
NPB_DBDGDHDF_40741
NPC_GIABBOKD_49399
NPB_DBDGDHDF_18622
NPA_FLPAEDJP_13546
RGC_MIPIHKEK_51134
NPA_FLPAEDJP_26129
NPC_GIABBOKD_07086
NPA_FLPAEDJP_20139
RGA_HMEDELBO_35087
NPA_FLPAEDJP_02313
NPB_DBDGDHDF_05392
NPC_GIABBOKD_03863
RGA_HMEDELBO_01145
RGB_AMJCBLCO_02649
RGC_MIPIHKEK_03960
RGB_AMJCBLCO_15241
RGC_MIPIHKEK_09207
RGA_HMEDELBO_09482
NPC_GIABBOKD_11812
NPB_DBDGDHDF_12077
ABW37061|Sphingomonas sp LH128|Bph
NP_049062|Novosphingobium aromaticivorans|Non
ACD91669|Novosphingobium sp H25|Non
CAT03469|Sphingomonas paucimobilis EPA505|Non
NPA_FLPAEDJP_12105
ACC64605|Sphingomonas sp B27|Phn
2GBW|Sphingomonas yanoikuyae B1|Bph
NPA_FLPAEDJP_41509
NPB_DBDGDHDF_12068
NPC_GIABBOKD_23271
RGA_HMEDELBO_09635
RGB_AMJCBLCO_25862
RGC_MIPIHKEK_09198
BAC81541|Cycloclasticus sp A5|Pap
ABF56510|Cycloclasticus sp P1|Pap
RGC_MIPIHKEK_90938
NPA_FLPAEDJP_18995
RGA_HMEDELBO_67647
NPC_GIABBOKD_26638
YP_008374307|Cycloclasticus zancles 7ME|Non
NPC_GIABBOKD_61959
RGB_AMJCBLCO_215453
RGC_MIPIHKEK_61232
ZP_06845988|Burkholderia sp Ch11|Non
RGB_AMJCBLCO_19118
ACG70971|Acidovorax sp NA3|Phn
NPC_GIABBOKD_21800
BAA76323|Alcaligenes faecalis AFK2|Phn
AAK62353|Burkholderia sp DBT1|DbtA
NPA_FLPAEDJP_20773
WP_007012495|Novosphingobium pentaromativorans|Non
WP_007014365|Novosphingobium pentaromativorans|Non
WP_007184423|Hydrocarboniphaga effusa|Non
BAD34447|Sphingomonas sp A4|Pap
AAD09872|Burkholderia sp RP007|Phn
YP_004468880|Alteromonas sp SN2|Non
YP_534822|Pseudomonas putida Nah7|Nah
NP_863072|Pseudomonas putida NCIB 98164|Nah
O07824|Pseudomonas fluorescens|Nah
Q51494|Pseudomonas aeruginosa|Nah
ADK11287|Pseudomonas stutzeri|Nah
2BMO|Comamonas JS765|Dnt
YP_987297|Acidovorax sp JS42|Non
ADQ90222|Pseudomonas stutzeri|Non
AAL50021|Burkholderia cepacia R34|Dnt
AAB09766|Burkholderia sp RASC|Dnt
YP_982710|Polaromonas naphthalenivorans CJ2|Non
ACT53249|Burkholderia sp C3|Pap
AAD12610|Ralstonia sp U2|Nah
ABX89315|Comamonas testosteroni|Nah
AAF72976|Comamonas testosteroni|Phn
YP_008372949|Cycloclasticus zancles 7ME|Non
YP_006838592|Cycloclasticus sp P1|Non
NPC_GIABBOKD_50599
NPB_DBDGDHDF_45217
NPA_FLPAEDJP_27567
RGB_AMJCBLCO_65706
RGC_MIPIHKEK_109304
NPC_GIABBOKD_50521
RGB_AMJCBLCO_15310
RGC_MIPIHKEK_09276
RGA_HMEDELBO_09413
NPC_GIABBOKD_28890
NPB_DBDGDHDF_12146
NP_049184|Novosphingobium aromaticivorans|Non
BAC65448|Sphingomonas sp P2|Bph
ABM79809|Sphingobium yanoikuyae|Bph
NPA_FLPAEDJP_42432
NPB_DBDGDHDF_19727
NPA_FLPAEDJP_39422
NPA_FLPAEDJP_05709
NPB_DBDGDHDF_12842
NPC_GIABBOKD_07127
RGA_HMEDELBO_33133
RGB_AMJCBLCO_42507
RGC_MIPIHKEK_19704
Cluster XXIV
Cluster XXVI
0.2
B
RGA_HMEDELBO_18959
RGB_AMJCBLCO_51308
NPC_GIABBOKD_31709
NPA_FLPAEDJP_11328
NPA_FLPAEDJP_23510
AAK16534|Arthrobacter keyseri|Pht
NPB_DBDGDHDF_30246
AFM73571|Arthrobacter sp 68b|Non
RGC_MIPIHKEK_118960
YP_001072483|Mycobacterium sp JLS|Non
ZP_05225089|Mycobacterium intracellulare ATCC 13950|Non
WP_010223641|Pseudonocardia sp P1|Non
BAC54156|Terrabacter sp DBF63|Pht
RGA_HMEDELBO_69184
RGB_AMJCBLCO_55218
WP_020540907|Nonomuraea coxensis|Non
WP_005444914|Saccharomonospora azurea|Non
WP_005050729|Microbacterium laevaniformans|Non
ZP_04747643|Mycobacterium kansasii ATCC 12478|Non
WP_019735208|Mycobacterium avium|Non
AAY57926|Rhodococcus sp TFB|Pht
AAR90178|Rhodococcus sp DK17|Pht
AAQ91914|Mycobacterium vanbaalenii PYR1|Pht
YP_951316|Mycobacterium vanbaalenii PYR1|Non
RGC_MIPIHKEK_103545
ZP_04749265|Mycobacterium kansasii ATCC 12478|Non
ZP_05223998|Mycobacterium intracellulare ATCC 13950|Non
ZP_06852460|Mycobacterium parascrofulaceum ATCC BAA614|Non
YP_882691|Mycobacterium avium 104|Non
RGA_HMEDELBO_58608
RGC_MIPIHKEK_50609
AAZ38356|Terrabacter sp HH4|Non
RGB_AMJCBLCO_114108
AAY85176|Mycobacterium vanbaalenii PYR1|Paa
AAZ78216|Mycobacterium sp CH2|Non
YP_951396|Mycobacterium vanbaalenii PYR1|Paa
BAA94708|Nocardioides sp KP7|Paa
AAQ12029|Mycobacterium sp S65|Non
CAD38647|Mycobacterium sp 6PY1|Paa
NPC_GIABBOKD_106588
YP_951339|Mycobacterium vanbaalenii PYR1|Paa
AAQ95210|Mycobacterium sp MCS|Non
BAD02377|Rhodococcus opacus SAO101|Non
ABH01029|Rhodococcus opacus R7|Nah
WP_017981165|Amycolatopsis methanolica|Non
ACV96857|Gordonia sp CCNAPH1296|Nah
AAD25395|Rhodococcus sp I24|Nah
YP_004243228|Arthrobacter phenanthrenivorans Sphe3|Non
RGA_HMEDELBO_24814
RGB_AMJCBLCO_139161
NPC_GIABBOKD_35844
NPA_FLPAEDJP_16092
NPB_DBDGDHDF_22627
RGC_MIPIHKEK_42793
Cluster V
Cluster I
Cluster II
0.3

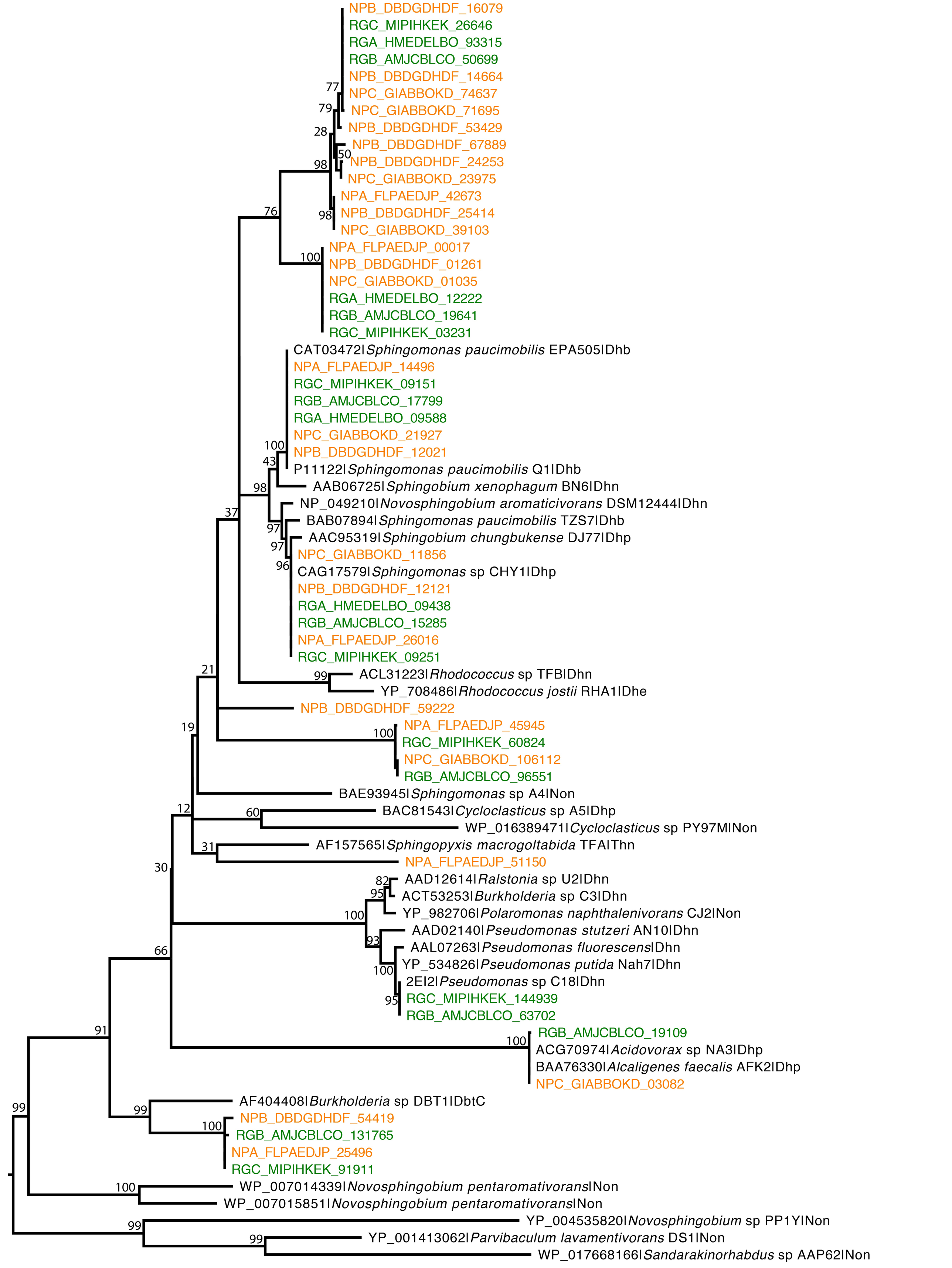
NPB_DBDGDHDF_16079
RGC_MIPIHKEK_26646
RGA_HMEDELBO_93315
RGB_AMJCBLCO_50699
NPB_DBDGDHDF_14664
77
NPC_GIABBOKD_74637
79
NPC_GIABBOKD_71695
NPB_DBDGDHDF_53429
28
NPB_DBDGDHDF_67889
50
98
NPB_DBDGDHDF_24253
NPC_GIABBOKD_23975
NPA_FLPAEDJP_42673
76
98
NPB_DBDGDHDF_25414
NPC_GIABBOKD_39103
NPA_FLPAEDJP_00017
100
NPB_DBDGDHDF_01261
NPC_GIABBOKD_01035
RGA_HMEDELBO_12222
RGB_AMJCBLCO_19641
RGC_MIPIHKEK_03231
CAT03472|Sphingomonas paucimobilis EPA505|Dhb
NPA_FLPAEDJP_14496
RGC_MIPIHKEK_09151
RGB_AMJCBLCO_17799
RGA_HMEDELBO_09588
NPC_GIABBOKD_21927
100
NPB_DBDGDHDF_12021
43
P11122|Sphingomonas paucimobilis Q1|Dhb
98
AAB06725|Sphingobium xenophagum BN6|Dhn
NP_049210|Novosphingobium aromaticivorans DSM12444|Dhn
37
BAB07894|Sphingomonas paucimobilis TZS7|Dhb
97
AAC95319|Sphingobium chungbukense DJ77|Dhp
97
NPC_GIABBOKD_11856
96
CAG17579|Sphingomonas sp CHY1|Dhp
NPB_DBDGDHDF_12121
RGA_HMEDELBO_09438
RGB_AMJCBLCO_15285
NPA_FLPAEDJP_26016
RGC_MIPIHKEK_09251
21
99
ACL31223|Rhodococcus sp TFB|Dhn
YP_708486|Rhodococcus jostii RHA1|Dhe
NPB_DBDGDHDF_59222
19
NPA_FLPAEDJP_45945
100
RGC_MIPIHKEK_60824
NPC_GIABBOKD_106112
RGB_AMJCBLCO_96551
BAE93945|Sphingomonas sp A4|Non
12
60
BAC81543|Cycloclasticus sp A5|Dhp
WP_016389471|Cycloclasticus sp PY97M|Non
31
AF157565|Sphingopyxis macrogoltabida TFA|Thn
NPA_FLPAEDJP_51150
30
82
AAD12614|Ralstonia sp U2|Dhn
95
ACT53253|Burkholderia sp C3|Dhn
100
YP_982706|Polaromonas naphthalenivorans CJ2|Non
AAD02140|Pseudomonas stutzeri AN10|Dhn
93
AAL07263|Pseudomonas fluorescens|Dhn
66
YP_534826|Pseudomonas putida Nah7|Dhn
100
2EI2|Pseudomonas sp C18|Dhn
95
RGC_MIPIHKEK_144939
RGB_AMJCBLCO_63702
91
RGB_AMJCBLCO_19109
100
ACG70974|Acidovorax sp NA3|Dhp
BAA76330|Alcaligenes faecalis AFK2|Dhp
NPC_GIABBOKD_03082
99
AF404408|Burkholderia sp DBT1|DbtC
99
NPB_DBDGDHDF_54419
100
RGB_AMJCBLCO_131765
NPA_FLPAEDJP_25496
RGC_MIPIHKEK_91911
100
WP_007014339|Novosphingobium pentaromativorans|Non
WP_007015851|Novosphingobium pentaromativorans|Non
99
YP_004535820|Novosphingobium sp PP1Y|Non
99
YP_001413062|Parvibaculum lavamentivorans DS1|Non
WP_017668166|Sandarakinorhabdus sp AAP62|Non
0.2

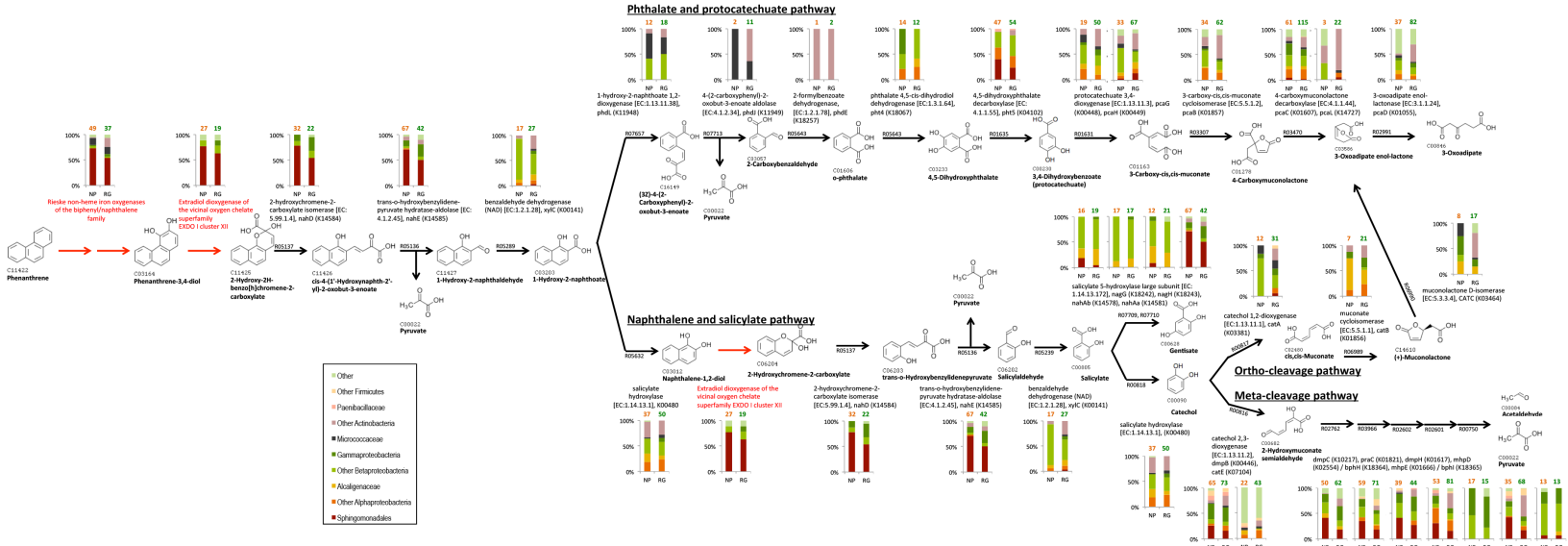
Phthalate and protocatechuate pathway
Naphthalene and salicylate pathway
Ortho-cleavage pathway
Meta-cleavage pathway
C11422
Phenanthrene
C03168
Phenanthrene-3,4-diol
C11425
2-Hydroxy-2H-benzo[h]chromene-2-carboxylate
C11426
cis-4-(1'-Hydroxynaphth- 2'-yl)-2-oxobut-3-enoate
C11427
1-Hydroxy-2-naphthaldehyde
C03203
1-Hydroxy-2-naphthoate
Rieske non-heme iron oxygenases of the biphenyl/naphthalene family
Extradiol dioxygenase of the vicinal oxygen chelate superfamily EXDO I cluster XII
2-hydroxychromene-2-carboxylate isomerase [EC: 5.99.1.4], nahD (K14584)
trans-o-hydroxybenzylidene-pyruvate hydratase-aldolase [EC: 4.1.2.45], nahE (K14585)
benzaldehyde dehydrogenase (NAD) [EC:1.2.1.28], xylC (K00141)
R05137
R05136
R05289
C00022
Pyruvate
1-hydroxy-2-naphthoate 1,2-dioxygenase [EC:1.13.11.38], phdL (K11948)
4-(2-carboxyphenyl)-2-oxobut-3-enoate aldolase [EC:4.1.2.34], phdI (K11949)
2-formylbenzoate dehydrogenase, [EC:1.2.1.78], phdE (K18257)
phthalate 4,5-cis-dihydrodiol dehydrogenase [EC:1.3.1.64], phd4 (K18067)
4,5-dihydroxyphthalate decarboxylase [EC: 4.1.1.55], pht5 (K04102)
protocatechuate 3,4-dioxygenase [EC:1.13.11.3], pcaG (K00448), pcaH (K00449)
3-carboxy-cis,cis-muconate cycloisomerase [EC:5.5.1.2], pcaB (K01857)
4-carboxymuconolactone decarboxylase [EC:4.1.1.44], pcaC (K01607), pcaL (K14727)
3-oxoadipate enol-lactonase [EC:3.1.1.24], pcaD (K01055),
R07657
R07713
R05643
R01635
R01631
R03307
R03470
R02991
C16149
(3Z)-4-(2-Carboxyphenyl)-2-oxobut-3-enoate
C03057
2-Carboxybenzaldehyde
C01606
o-phthalate
C03233
4,5-Dihydroxyphthalate
C08239
3,4-Dihydroxybenzoate (protocatechuate)
C01163
3-Carboxy-cis,cis-muconate
C01179
4-Carboxymuconolactone
C00966
3-Oxoadipate enol-lactone
C00946
3-Oxoadipate
R05632
C03012
Naphthalene-1,2-diol
C06204
2-Hydroxychromene-2-carboxylate
R05137
C06203
trans-o-Hydroxybenzylidenepyruvate
R05136
C00022
Pyruvate
C06202
Salicylaldehyde
R05239
C00805
Salicylate
R07709, R07710
C00628
Gentisate
R00818
C00090
Catechol
salicylate hydroxylase [EC:1.14.13.1], K00480
Extradiol dioxygenase of the vicinal oxygen chelate superfamily EXDO I cluster XII
2-hydroxychromene-2-carboxylate isomerase [EC:5.99.1.4], nahD (K14584)
trans-o-hydroxybenzylidene-pyruvate hydratase-aldolase [EC:4.1.2.45], nahE (K14585)
benzaldehyde dehydrogenase (NAD) [EC:1.2.1.28], xylC (K00141)
salicylate 5-hydroxylase large subunit [EC: 1.14.13.172], nagG (K18243), nagH (K18243), nahAb (K14578), nahAa (K14581)
salicylate hydroxylase [EC:1.14.13.1], (K00480)
catechol 1,2-dioxygenase [EC:1.13.11.1], catA (K03381)
muconate cycloisomerase [EC:5.5.1.1], catB (K01856)
muconolactone D-isomerase [EC:5.3.3.4], CATC (K03464)
R00817
R06989
C01489
cis,cis-Muconate
C14610
(+)-Muconolactone
R00816
catechol 2,3-dioxygenase [EC:1.13.11.2], dmpB (K00446), catE (K07104)
2-Hydroxymuconate semialdehyde
C00940
dmpC (K10217), praC (K01821), dmpH (K01617), mhpD (K02554) / bphH (K18364), mhpE (K01666) / bphI (K18365)
R02762
R03966
R02602
R02601
R00750
C00024
Acetaldehyde
C00022
Pyruvate
Other
Other Firmicutes
Paenibacillaceae
Other Actinobacteria
Micrococcaceae
Gammaproteobacteria
Other Betaproteobacteria
Alcaligenaceae
Other Alphaproteobacteria
Sphingomonadales
NP
RG